Of particular interest from [R8-41]

8-43. Mott, N. F., "On the Oxidation of Silicon," *Phil. Mag.*, **55**, 117 (1987).
8-44. Leroy, B., "Stresses and Silicon Interstitials during the Oxidation of a Silicon Substrate," *Phil. Mag.*, **55**, 159 (1987).
8-45. Blanc, J., "The Oxidation of Silicon by Dry Oxygen. Can We Distinguish between Models?," *Phil. Mag.*, **55**, 685 (1987).

CHAPTER 9

MICROLITHOGRAPHY

9-1 MICROSTRUCTURE FABRICATION

Although microelectronic devices are three dimensional, they are fabricated largely by *planar processes*. By this phrase we mean that the geometry is "written" onto a planar substrate (the wafer) and upon subsequent planar films such as oxide layers. To carry the writing analogy further we must note that the "ink" with which the various features are written is usually thick relative to the width of the lines being written. It is through the line thickness that the three-dimensional structure is created.

Microstructures of interest to us have features whose minimum dimensions are in the range of 0.1–1 μm. To create such microstructures it is necessary that three tools or processes be available:

1. We must have a *writing tool* whose "point" is small compared to the width of the line being written. Only in this way can the feature line width be precisely controlled. The most common writing tools are optical and electron beams. The latter is capable of writing a line less than 100 Å wide.
2. We must be able to *record* the pattern of the radiation on the substrate. This requires a radiation-sensitive material and a means of depositing that material onto the substrate for recording. For reasons that will be clear shortly, this material is called a "resist." Most resists are polymeric films whose molecular weight can be altered by radiation absorption.
3. The pattern written onto the resist must be converted, or *developed*, into a mask or stencil. The desired structural feature is then created on the substrate, either by

depositing a material (such as an oxide or a metal) or removing the underlying material (e.g., by etching), in either case through the open area of the mask.

The manipulation of the writing tool together with the application and development of the resist make up the process that we call *microlithography*.

Figure 9-1 outlines the steps involved in microlithography. A designer creates a *mask*, which contains the pattern that is to be replicated on the wafer surface. In the most common examples, the pattern ultimately is fabricated onto the semiconductor surface by the processes of deposition or etching—addition or removal of material from the surface. Lithography is the technique whereby specific areas of the surface, according to the desired pattern, are opened to deposition or etching.

In the most frequently used methods, one begins by placing a thin layer of protective or resistant material, *photoresist*, onto the wafer surface. This is usually accomplished by coating the photoresist, in liquid form, onto the wafer. *Spin coating*,

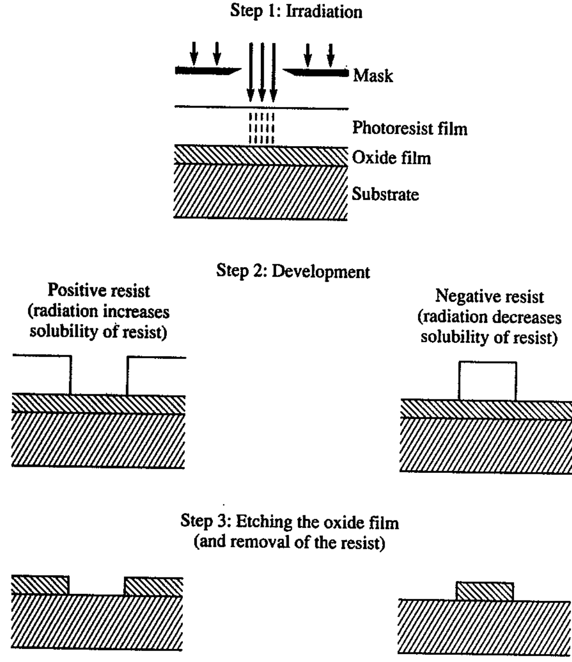

FIGURE 9-1
Creating features with positive and negative resists. Note that different masks must be used with positive and negative resists in order to create identical features. In the case shown here, the same mask yields different features.

the prevalent method, typically produces very uniform films of about 1 μm thickness, after solvent evaporation and hardening (by baking) of the film.

The film is irradiated through the mask, using photons (photolithography), electrons (*e*-beam lithography), or x-rays (x-ray lithography). The photoresist reacts chemically in the exposed areas and, depending upon the choice of chemical system, will become more soluble or less soluble with respect to some solvent. (A *positive* resist is one that reacts to become *more* soluble.) The image, the area exposed to radiation, is then developed. In a positive resist, the exposed regions are dissolved, and the remaining resist film replicates the mask. The opposite, of course, is the case for a negative resist. The term *development* refers to dissolution of the resist material. Figure 9-1 illustrates these ideas.

In the next step, following development and using etching as the example, the exposed area of the wafer—the area from which the resist has been dissolved—is etched either by a wet chemical step or by dry methods such as plasma or reactive ion etching. Finally, the remaining resist film must be removed. This is usually accomplished by etching with plasma or reactive ions, and/or liquid dissolution with solvents. This sequence may be repeated many times in order to lay down into the etched regions films or lines of various materials such as conductors, or to define regions which, in subsequent steps, will contain precise patterns of various dopants.

One measure of the importance of lithography in semiconductor fabrication is the fraction of process time devoted to the lithographic steps of resist application, exposure, development, and cleaning prior to the next step. One estimate [R9-3] attributes 60% of process time to lithography.†

We do not consider the optical or imaging problems of lithography in any detail here. Of special interest to us, however, are the following topics:

1. The organic and physical chemistry of polymers—the most commonly used class of resist materials—and, in particular, the effect of radiation on polymer molecular weight.
2. The kinetics and the uniformity of the dissolution (development) process.
3. The spin coating process, especially the factors that determine film thickness and film uniformity, and the relationship of processing parameters such as spin speed and duration and solution rheology to final film thickness.

Much of the data used in illustrations of the topics that follow involve the use of electron-beam radiation. Current technology uses *e*-beam radiation to manufacture masks, while optical (UV) radiation is used more commonly to expose the patterns on the wafers. The difference lies largely in the magnitude of the radiant energy densities, but the principles and techniques illustrated here are appropriate to both radiation sources.

†The other 40% is ascribed to "hot processes"—oxidation, doping, CVD (21%)—testing (8%), metallization (7%), and ion implantation (4%).

9-2 SOME ASPECTS OF ORGANIC RESIST MATERIALS

To be useful in semiconductor applications, a resist material must have a controllable response to radiation as well as the ability to allow optical resolution of very small features. The resist must be available in a solution that permits spin coating into a thin, uniform, continuous film that adheres to a variety of solid surfaces and withstands exposure to high-temperature and corrosive etching environments without loss of line definition.

Both positive and negative photoresists can be classified as one- or two-component systems. A one-component system is usually based upon a polymer that undergoes a photochemical reaction; in a two-component system a sensitizer molecule (monomeric) is dissolved in an inert polymeric matrix. The sensitizer undergoes the photochemical reaction.

A common positive photoresist consists of a phenolic resin matrix and a diazonaphthoquinone sensitizer, and so is a two-component system. Polymethyl methacrylate (PMMA) is a classical one-component positive resist that has intrinsic radiation sensitivity. In PMMA, exposure to *e*-beam, x-ray, or gamma radiation causes chain scission, reduced molecular weight, and enhanced solubility.

9-2.1 Examples of Resist Chemistry

(a) Two-component negative resist:
Matrix resin: synthetic rubber (poly *cis*-isoprene)
Sensitizer: bisazide
The bisazide sensitizer under radiation gives nitrine + nitrogen:

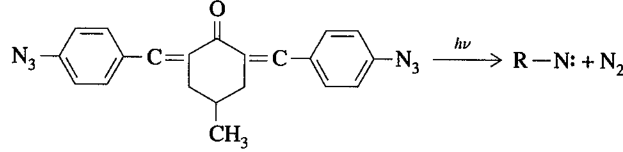

The nitrines react to produce polymer-polymer linkages and three-dimensional cross-linked structures that are less soluble in the developer solution:

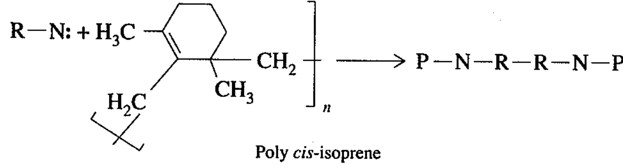

Poly *cis*-isoprene

(b) Two-component positive resist:
Matrix resin: phenol-formaldehyde copolymer (novolak)
Sensitizer: diazoquinone

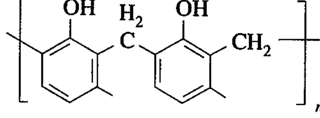

The sensitizer is randomly distributed in the polymer matrix. Exposure to radiation renders matrix regions locally soluble in base.

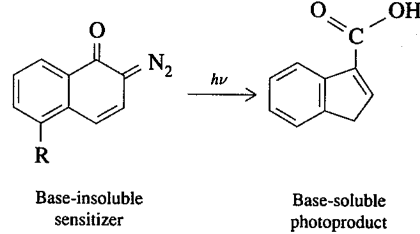

(c) One-component positive resist:
Polymer: polybutene-1-sulfone

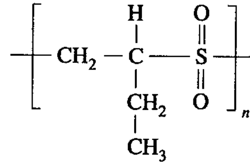

Radiation leads to chain scission, and hence a reduced molecular weight. This produces a more soluble material:

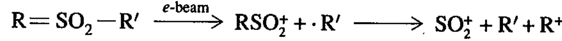

$$R{=}SO_2{-}R' \xrightarrow{e\text{-beam}} RSO_2^{+} + \cdot R' \longrightarrow SO_2^{+} + R' + R^{+}$$

(d) One-component negative resist:
Polymer: copolymer of glycidyl methacrylate and ethyl acrylate

$$\left[-CH_2-C(CH_3)(C(=O)O-CH_2-\text{epoxy})-CH_2-C(H)(C(=O)O-CH_2-CH_3)-\right] \quad \text{or} \quad R-CH-CH_2 \text{ (epoxide, O bridging)}$$

(active element is the epoxy group)

A crosslinking reaction is initiated by *e*-beam radiation in the presence of an anion:

$$A^- + R-\overset{O}{CH-CH_2} \xrightarrow{e\text{-beam}} R-\underset{CH_2A}{CH}-O^-$$

This propagates to lead to insoluble high-molecular-weight material:

$$R-\underset{CH_2A}{CH}-O^- + R-\overset{O}{CH-CH_2} \xrightarrow{e\text{-beam}} R-\underset{CH_2A}{CH}-O-CH_2-\underset{R}{CH}-O^-$$

We do not deal further with the chemical details that distinguish and thus recommend one type of photoresist with respect to another. Subsequent comments are directed primarily to one of the commonest polymeric materials studied as a resist—polymethyl methacrylate (PMMA), a one-component positive photoresist:

$$\left[-\underset{H}{\overset{H}{C}}-\underset{C(=O)-O-CH_3}{\overset{CH_3}{C}}-\right]$$

PMMA behaves in a manner similar to polybutene-1-sulfone, described previously. Radiation leads to chain scission of PMMA with evolution of CO_2.

9-2.2 Resist Sensitivity to Radiation

When radiation interacts with the molecules in a polymeric film, the events that result can be described quantitatively by the number of events (chain scission, crosslinking, radical evolution, etc.) per unit of absorbed energy. We usually refer to this as the *radiation chemical yield G*. The amount of incident energy is usually referred to as a *dose D*. Because different systems of units are used to describe radiation in different sources we must be prepared to convert units when referring to and comparing one published study to another.

The electron volt is frequently used as the unit of energy, so we begin by recalling that one electron volt (1 eV) is the energy acquired by an electron accelerated through a potential difference of one volt (1 V). Since the charge on one electron is 1.6022×10^{-19} coulombs (C), the energy is calculated as

$$1 \text{ eV} = (1.6022 \times 10^{-19} \text{ C}) \times 1 \text{ V} = 1.6022 \times 10^{-19} \text{ joule (J)} \tag{9-1}$$

(The precision with which this number is known far exceeds the precision appropriate to engineering calculations. We generally write this as 1.6, rather than 1.6022.)

Sometimes we find radiation units reported as rads, so we must know that, by definition,

$$1 \text{ rad} = 6.25 \times 10^{13} \text{ eV/g} \tag{9-2}$$

Note that the rad is a "specific" energy in units of energy per *mass*.

We also find radiation doses reported for electron beam (*e*-beam) radiation in units of coulomb per square centimeter (C/cm^2). But the coulomb is a unit of *charge*, not energy. This is a very confusing feature of the literature on lithography. It arises because different forms of radiation (x-ray, γ-ray, and *e*-beam) are absorbed to differing degrees in a polymeric resist medium. Very little of the incident *e*-beam radiation is absorbed by polymeric resists under conditions typical of lithography. As a consequence, one normally finds *e*-beam radiation characterized by the *emitted* or *incident* dose of energy. This is typically measured by an instrument that detects the *charge* that accumulates on a target placed in the beam, hence the units of C/cm^2. We will find, then, that when an area of resist film is exposed to (irradiated by) an electron beam, the "strength" of the beam—the *dose*—is usually stated in terms of the *incident charge per unit of area*. The most commonly used units are actually microcoulombs per square centimeter ($\mu C/cm^2$). But this incident charge density is not related in a unique way to the electron energy that is actually dissipated within, i.e., *absorbed by*, the volume of the resist material. The fraction of the energy absorbed depends upon the accelerating voltage of the beam and upon the resist film thickness.

Theoretical studies of electron energy dissipation are available [R9-5,6]. Figure 9-2 shows calculations of Hatzakis et al. [R9-5] for PMMA films on silicon substrates. We know of no similar calculations for other polymeric resists. Note that nearly all of the energy incident in a low-energy electron beam is absorbed, especially in a thick film. High-energy electrons, however, can simply pass through a thin polymer film without much interaction (absorption). For high-energy radiation (> 20 keV) upon thin films (< 1 μm) the fraction of energy absorbed becomes independent of the beam intensity.

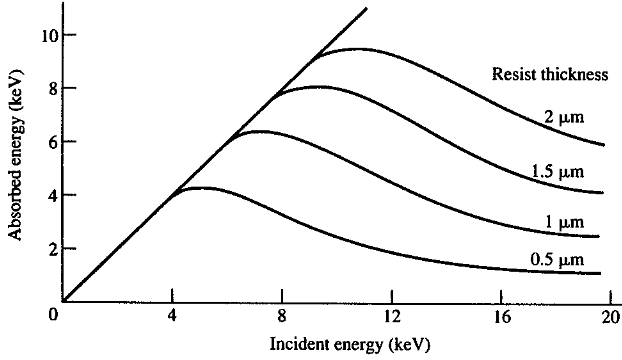

FIGURE 9-2
Relationship of absorbed to incident *e*-beam energy in thin films of PMMA on a silicon substrate.

Since *e*-beam dose is commonly reported as μC/cm^2 *incident energy*, we must have a means of converting this *areal* (flux) unit to *volumetric absorbed energy* (eV/cm^3) and vice versa. To do this we need the charge on an electron (1.6×10^{-19}C) and we recall that one joule (1 J) is one volt-coulomb (1 VC). The conversion is performed using the following expression:

$$\frac{\mu\text{C/cm}^2}{\text{eV/cm}^3} = \frac{E_a(\text{eV}) \times 10^{-6}}{H(\text{cm})} \times \frac{1}{1.6 \times 10^{19}(\text{J/eV})} = 6.25 \times 10^{12}\frac{E_a(\text{eV})}{H(\text{cm})} \tag{9-3}$$

where H is the resist film thickness in cm units. The use of this conversion is illustrated in Example 9-2.1.

When a polymer is irradiated with a specific dose D, in electron volts per gram of polymer, the total number N^* of scissions produced is observed to obey

$$N^* = KDw \tag{9-4}$$

where w is the mass of polymer and K is a molecular (structural) parameter. One normally replaces K with the so-called G value:

$$G = 100K \tag{9-5}$$

G is the number of chain scissions produced per 100 eV of *absorbed* energy. (It is the radiation chemical yield for chain scission.)

We define the number average molecular weight by

$$M_n^\circ = \frac{wN_A}{N_0} \tag{9-6}$$

where N_0 is the number of molecules in a sample of mass w and N_A is Avogadro's number. After exposure to a dose, the number average molecular weight changes to

$$M_n = \frac{wN_A}{N_0 + N^*} \tag{9-7}$$

(Each chain scission produces *one* additional molecule.) This can be rearranged to the form

$$\frac{1}{M_n} = \frac{1}{M_n^\circ} + \frac{G}{100N_A}D \tag{9-8}$$

Confirmation of this model is presented in Figure 9-3 for electron beam radiation. Sensitivity to radiation is usually measured by the G value, and hence by the slope of plots as in Figure 9-3. A large G value means that the variation in molecular weight is much more sensitive to variations in radiation dosage. This ultimately gives better definition of features.

Example 9-2.1 e-Beam dose requirement. An electron beam is available, with a thermionic gun that puts out a current density of 10 A/cm^2 in a 0.1-μm-diameter spot on the target. If a PMMA resist is used, Figure 9-3 may be used to characterize the resist. Find (*a*) the G value and (*b*) the exposure time required to reduce the number average molecular weight from its initial value to 20,000.

First we examine Figure 9-3. The $D = 0$ intercept gives $1/M_n^\circ \times 10^6 = 8$, or $M_n^\circ = 125{,}000$. From the slope of the line and Eq. 9-6 we find

$$\frac{G}{100N_A} = 2.1 \times 10^{-6} \qquad (\text{with } D \text{ in } \mu\text{C/cm}^2) \tag{9-9}$$

Since G is normally given in units of eV, we must perform a conversion of units. But, as just discussed, what we really need, in addition to a unit conversion, is also the fraction of *e*-beam energy that is *absorbed* by the PMMA resist. We may use Figure 9-2, but we need information on the incident energy of the beam and on the resist thickness. Let us assume that we are using a 25 keV machine on a 1 μm resist. From Figure 9-2 we find that the absorbed energy is about 2.5 keV.

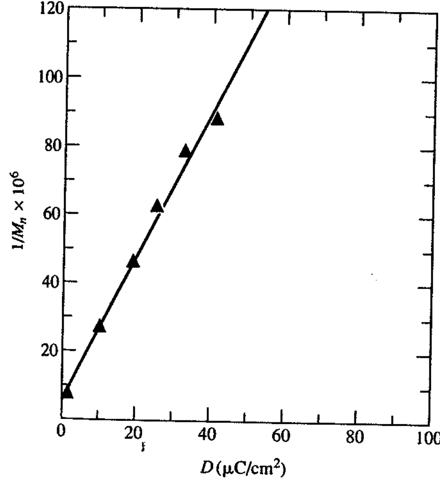

FIGURE 9-3
Inverse molecular weight as a function of *e*-beam dose for PMMA.

With the conversion factor from Eq. 9-3 and the resist thickness $H = 1\ \mu$m we may calculate

$$\frac{\mu\text{C/cm}^2}{\text{eV/cm}^3} = \frac{6.25 \times 10^{12}(2.5 \times 10^3 \text{ eV})}{(10^{-4} \text{ cm})} = 1.6 \times 10^{20} \quad (9\text{-}10)$$

From Eq. 9-9 we now find

$$G = \frac{2.1 \times 10^{-6}(100)6.023 \times 10^{23}}{1.6 \times 10^{20}} = 0.8 \text{ scissions/100 eV} \quad (9\text{-}11)$$

We assume that G is independent of M_n so that we can use the same G value for $M_n^\circ = 125{,}000$. Then, from Eq. 9-6,

$$\frac{1}{20{,}000} = \frac{1}{125{,}000} + 2.1 \times 10^{-6} D \quad (9\text{-}12)$$

or $D = 20\ \mu\text{C/cm}^2$. Since the thermionic gun puts out $10\text{A/cm}^2 = 10C/(\text{cm}^2 \cdot \text{s})$, the required exposure time is $20 \times 10^{-6}/10 = 2\ \mu$s.

9-2.3 Resist Sensitivity to Development

In a positive resist such as PMMA chain scission gives a reduced molecular weight, thereby producing a film that is more easily dissolved by a selected solvent. The term *development* refers to the dissolution and removal of the more soluble regions of the resist film. In this section we consider the factors that control the kinetics of dissolution.

Figures 9-4 and 9-5 show two important aspects of resist development. In Figure 9-4 [R9-1] we see that relatively small changes in the incident radiation density can have a significant effect on the postdevelopment resist profile in a common positive polymeric material such as PMMA. Figure 9-5 [R9-34] shows the kinetics of development—the temporal evolution of resist profiles under a given set of development conditions. To understand and model such results, several pieces of information must be gathered and put together:

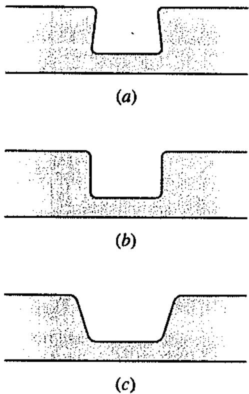

FIGURE 9-4
Resist profiles in PMMA at incident charge densities of (*a*) 10^{-4} C/cm², (*b*) 8×10^{-5} C/cm², and (*c*) 5×10^{-5} C/cm².

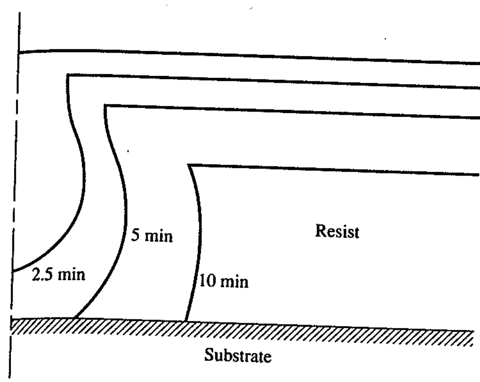

FIGURE 9-5
Time evolution of resist profiles in PMMA.

1. The effect of radiation on molecular weight must be known. Equation 9-8 gives an appropriate model of this phenomenon.
2. The spatial distribution of *absorbed* radiation must be related to the *incident* radiation and the absorptive and reflective characteristics of the resist and the substrate. The volume of resist, even if exposed to uniform incident radiation, does not show uniform absorption of radiation. Hence there will be a *spatial distribution* of chain scission within the resist.
3. The dependence of solubility on molecular weight must be known. Considering the remarks in 2 above, there will be a solubility distribution within the exposed region. Hence the contours do not replicate a rectangular geometry, as Figure 9-4 clearly shows.

When these pieces of information are available and properly integrated, it is possible to produce a mathematical model of the kinetics of dissolution (development). Prior to describing an approach to such modeling, we begin by examining some features of dissolution kinetics. Data may be obtained by creating samples of resist film over a relatively large surface, so that the distribution of both incident and absorbed radiation is spatially homogeneous. The resulting resist may then be dissolved in a bath, or stream, of solvent, and data on remaining film thickness as a function of time may be obtained. Figure 9-6 shows such a set of data. In this case, *e*-beam radiation is used to break molecular chains in the (positive) polymer resist.

One important feature of such data is the *sensitivity* of the resist–developer system, which may be defined by plotting the data from Figure 9-6 into the form of

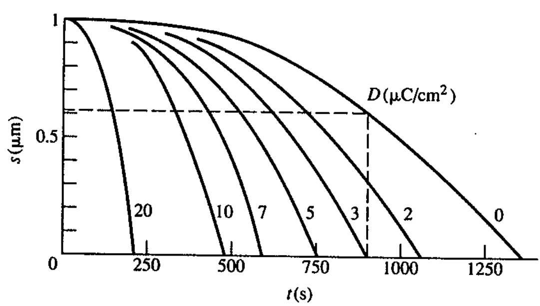

FIGURE 9-6
Rate of dissolution as a function of e-beam dose.

Figure 9-7.† For a particular dose (say, 3 μC/cm^2) we may find the time to remove a 1-μm film (about 900 s, from Fig. 9-6). At that time, the unexposed (i.e., zero-dose) region of the film is 0.62 μm thick. Data are then plotted as thickness *remaining* (of unexposed resist) as a function of dose.

If one draws a straight line through the data, as shown, an intercept of that line with the value of the original film thickness may be used to define a dose labeled D_s, as shown. One usually refers to D_s as a measure of the sensitivity of the resist. Films

†This should be the same as fig. 11, p. 105, of [R9-1]. We believe the x axis of that figure is mislabeled.

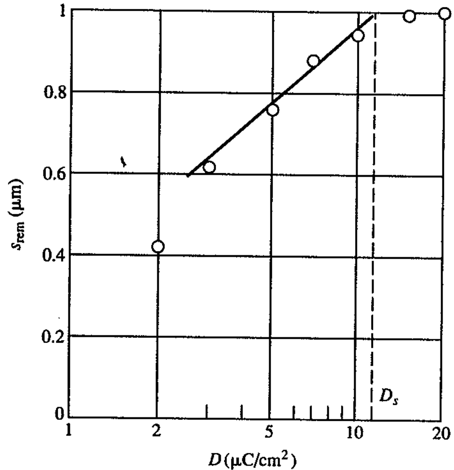

FIGURE 9-7
Sensitivity curve corresponding to Figure 9-6, where s_{rem} is thickness remaining.

with a *low* D_s are said to be the *more* sensitive. In addition to the intercept D_s, the *slope* of the linear portion of the line in Figure 9-7 is sometimes used to define what is called the *contrast* of the resist. A steep slope corresponds to *high* contrast, since a relatively small difference in dose gives rise to a large difference in dissolution rate.

Example 9-2.2 Development sensitivity of a positive resist. By way of example, suppose that the rate of removal of resist film obeys the relationship

$$-\frac{ds}{dt} = \beta M_n^{-\alpha} \tag{9-13}$$

The term $-ds/dt$ is the rate of change in resist film thickness (the disolution rate) and Eq. 9-13 is simply an empirical expression of the observation that polymer dissolution is an inverse power function of molecular weight. We will use Eq. 9-8 to relate M_n to the radiation dose, for a positive resist. With this model we may examine the sensitivity of a resist that obeys Eq. 9-13.

We will draw figures corresponding to Figures 9-6 and 9-7 for the resist described by Eq. 9-13, using the following parameters (when ds/dt is in units of Å/min and D is in μC/cm^2):

$$\beta = 4 \times 10^{12} \qquad \alpha = 2$$

$$M_n^\circ = 10^5 \qquad \frac{G}{100N_A} = 2.1 \times 10^{-6}$$

Our model takes the form

$$-\frac{ds}{dt} = \beta\left[\frac{1}{M_n^\circ} + \frac{G}{100N_A}D\right]^\alpha \tag{9-14}$$

or

$$-\frac{ds}{dt} = 4 \times 10^{12}\left(10^{-5} + 2.1 \times 10^{-6}D\right)^2 \tag{9-15}$$

Assuming an initial film thickness of 1 μm we may generate Figure 9-8 since, from Eq. 9-15,

$$s = s_0 - 400(1 + 0.21D)^2 t \tag{9-16}$$

where s and t are in units of Å and min. (Note that in Fig. 9-8 time is shown in *seconds* to parallel Fig. 9-7.) In this example we use $s_0 = 10^4$ Å $= 1$ μm.

We may define a development time t_{dev} as the time required to dissolve 1 μm of resist. Then, from Eq. 9-16,

$$t_{dev} = \frac{10^4}{400(1 + 0.21D)^2} \tag{9-17}$$

Note that here t_{dev} is defined as a function of D through Eq. 9-17. Figure 9-8 gives the thickness remaining for an undosed resist ($D = 0$) after the time t_{dev}. This follows from Eq. 9-16, setting $D = 0$, so that

$$s_{rem} = s(t_{dev}) = 10^4 - 400t_{dev}(D) \qquad \text{for each value of } D \tag{9-18}$$

This yields Figure 9-9. Note that the "linear" region has a slope that depends upon the choice of data points used to define the line. (This was also the case in Fig. 9-7.) Hence the definition of D_s (sensitivity) through an extrapolation from the slope of the data, when plotted in the semilog coordinates of Figure 9-7, is not unequivocal. It makes more

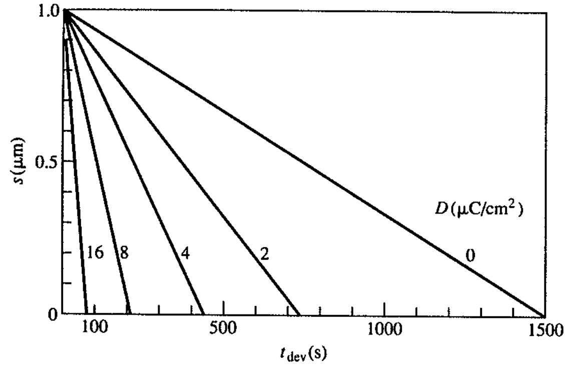

FIGURE 9-8
Development curve for Example 9-2.2.

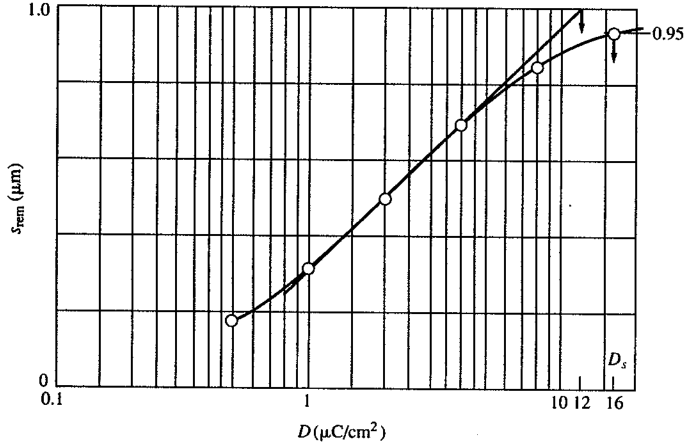

FIGURE 9-9
Sensitivity curve for Example 9-2.2.

sense to define D_s as the dose at which nearly all (say, 95%) of the initial (undosed) film remains after all of the dosed film is dissolved. From Figure 9-9 we find a value of sensitivity (D_s) of 16 μC/cm^2. If there were no linear portion at all in Figure 9-9, we could not define the contrast by the slope. This example points out how parameters can be model-dependent, and hence not definable in some situations.

For a *negative* resist, we may also define the properties of sensitivity and contrast through an exposure/development experiment. Normally, a negative resist is com-

pletely soluble to a specific developer prior to exposure. At a sufficiently large dose of radiation the resist is so thoroughly crosslinked through photochemical reaction that the film is *insoluble* in the developer. Figure 9-10 is a "sensitivity plot" for a negative resist.

For a given dose, *and at some fixed development time*, the film thickness that remains undissolved after exposure to solvent for that fixed time behaves typically as shown. Until the dose exceeds some minimal value D_g^i, called the *gel dose*, the film is so low in molecular weight that it is entirely dissolved. At and above some large dose D_g^* no solubilization occurs during the time of development. When the data are plotted as *normalized* film thickness after development against the logarithm of dose, and a straight line is drawn through the data as shown, it is possible to define a dose D_g° (near but less than D_g^*), as seen in Figure 9-10. One measure of sensitivity is the value of the dose D_g°.

The *contrast* of a negative resist is usually defined as

$$\gamma_n = \left(\log \frac{D_g^\circ}{D_g^i}\right)^{-1} \tag{9-19}$$

Contrast is an important feature of a resist because it is a measure of how strongly the dissolution rate changes with a variation in dose. Because the optics of irradiation and transmission of the incident beam are not perfect, the intended dosed and undosed regions are actually separated by a region with a gradient of absorbed dose. Hence there is a solubility gradient rather than an abrupt plane of demarcation between soluble and insoluble resist. The greater the contrast, the sharper the gradient, with the

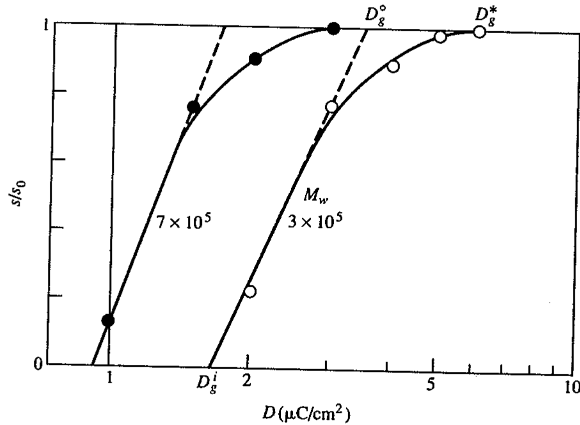

FIGURE 9-10
Sensitivity curves for a negative resist, poly(*p*-chlorostyrene), at two molecular weights. Note the definitions of D_g^i, D_g°, and D_g^*.

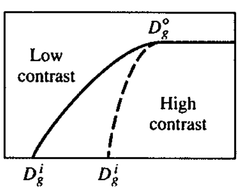

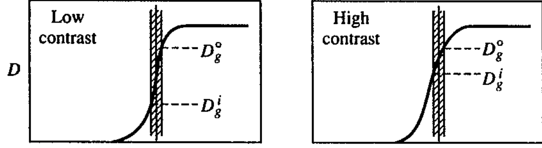

FIGURE 9-11
The effect of contrast.

result that the boundary of the developed volume of photoresist can be more precisely placed. This idea is illustrated schematically in Figure 9-11. Under idealized conditions there is a sharp radiation "shadow" under the mask that separates "night" from "day" and hence produces a sharp boundary between completely soluble and insoluble resist. Development yields a substrate that is bare right up to the shadow or mask line. Under real conditions radiation intrudes laterally into the resist under the mask. Although the dose received in that region may be low, there will be a "twilight" region in which some crosslinking of the resist can occur. If the doses D_g^i and D_g° are far apart (low contrast), there will be a region of substantial thickness which develops more slowly than unradiated resist, and so a relatively broad region of some undeveloped resist will remain on the substrate under the geometrical shadow of the mask. In a high-contrast resist, for which D_g^i is close to D_g° (and so γ is large), the lateral distance over which the resist film falls from its full thickness to the bare substrate will be very small. Hence a high-contrast resist permits a more precise placement of the line of demarcation of the bare substrate from the resist-protected region of the substrate.

Example 9-2.3 Contrast and sensitivity of a negative resist. The data presented in Figure 9-10 are for a styrene-based polymer, PCS, poly(p-chlorostyrene), whose monomer structure is

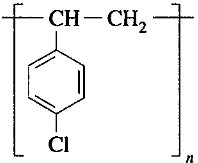

PCS is a negative photoresist. Give values of contrast γ_n and sensitivity (defined by D_g°) for the two different molecular weight samples of PCS studied.

We begin by drawing a straight line through the data, as shown. The intercepts on the dose axis define values of D_g^i and D_g° (in units of μC/cm^2). From Eq. 9-19 the contrast follows as

$$\gamma_n = \left(\log \frac{D_g^\circ}{D_g^i}\right)^{-1} \tag{9-20}$$

$$= \left(\log \frac{1.7}{0.92}\right)^{-1} = 3.8 \quad \text{for } M = 700{,}000 \tag{9-21}$$

$$= \left(\log \frac{3.5}{1.7}\right)^{-1} = 3.2 \quad \text{for } M = 300{,}000 \tag{9-22}$$

It appears that the contrast is not a strong function of molecular weight.

Obviously the sensitivity values, as defined by D_g°, are strongly molecular weight–dependent, and we find

$$D_g^\circ = 1.7\ \mu\text{C/cm}^2 \quad \text{for } M = 700{,}000 \tag{9-23}$$

$$= 3.5\ \mu\text{C/cm}^2 \quad \text{for } M = 300{,}000 \tag{9-24}$$

A *positive* resist can be treated in a manner entirely parallel to that just described for a negative resist. Instead of plotting the dissolution data as in Figure 9-7, where the thickness of the *undosed* film is plotted, we can plot the thickness of the *dosed* region, relative to its initial value, as a function of dose. Then we obtain a figure as shown in Figure 9-12 [R9-13]. The dose D_p gives the *sensitivity* of the resist, while

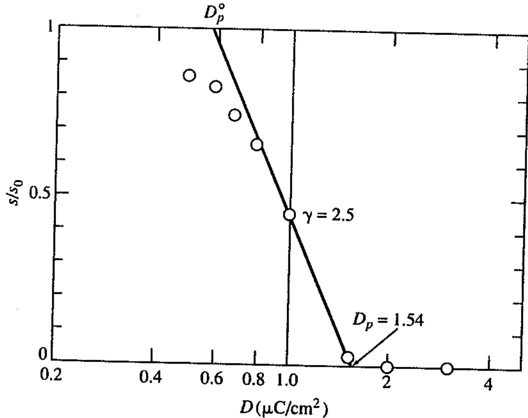

FIGURE 9-12
Sensitivity plot for a positive resist.

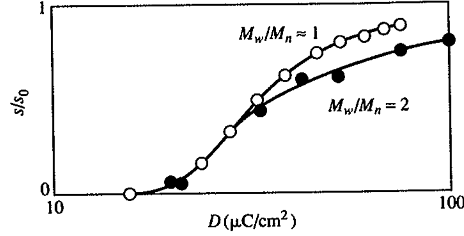

FIGURE 9-13
Effect of molecular weight distribution on sensitivity curves of a polystyrene resist.

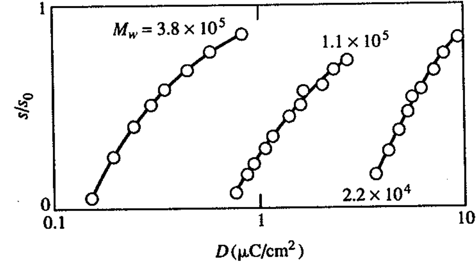

FIGURE 9-14
Effect of average molecular weight on sensitivity curves of a chlorinated polystyrene resist.

the contrast is defined by

$$\gamma_p = \left(\log \frac{D_p}{D_p^\circ}\right)^{-1} \tag{9-25}$$

One problem with the foregoing definitions of contrast (and to some degree of sensitivity) is that it is assumed that development data, when plotted as described, do show a well-defined linear region. A clear example of the failure of this assumption, for a negative resist, can be seen in the data of Feit and Stillwagon [R9-11] presented in Figure 9-13. These authors do give values for the contrast parameter γ for each polymer, but in their discussion they refer to γ as "the slope of the 'linear' portion of the characteristic curve." By putting the word *linear* in quotation marks, these authors provide one of the few published admissions that the linear region is not always well defined.

In an attempt to produce better resists, there have been many studies of the effect of polymer structural characteristics on resist performance. Figure 9-14 [R9-1] shows one aspect of this, for a negative resist. The sensitivity is clearly a strong function of the weight average molecular weight M_w. (In all three polymer samples the ratio M_w/M_n is held constant.) On the other hand, the contrast (the "slope" of these curves) is, although difficult to define clearly, apparently not a function of molecular weight.

9-3 THE KINETICS OF DEVELOPMENT

Parameters such as sensitivity and contrast are ultimately connected to the molecular structure of the polymer and to the solution used as the developer. This is true, as well, of the *rate* at which development proceeds. Thus any model of resist development

must ultimately be based on the dynamics of polymer dissolution. Hence we begin with a physical picture of a dissolving polymer [R9-27, 28]. Figure 9-15 depicts some of the relevant ideas. Dissolution begins as solvent molecules diffuse into the glasslike polymer phase. The solvated polymer *swells* somewhat, and the swollen region adjacent to the solution is called a *gel*. Within this region, which may be regarded as a highly concentrated solution, polymer molecules become less entangled than they are in the glassy region, and then increasingly mobile, permitting them to diffuse toward the development solvent-gel boundary. This boundary may be defined as the surface that separates free from entangled polymer chains. It is defined by a critical concentration that is characteristic of the polymer-solvent pair and the polymer molecular weight. For the concentration variable we use the polymer volume fraction C_{pd}^* here. The rate at which polymer molecules disentangle from the gel and become free is a complex function of polymer and solvent properties. We denote this rate by R and identify it with the dissolution rate $-ds/dt$. Figure 9-16 shows concentration profiles in the gel region. Volume fractions are initially unity (by definition) for polymer and solvent in their respective phases. Adjacent to the solvent-gel interface (on the solution side) we allow for the possibility of a diffusion boundary layer. This may add

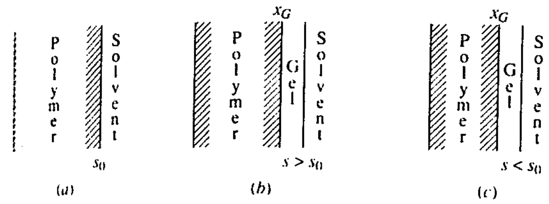

FIGURE 9-15
Kinetics of polymer dissolution. (*a*) Initial glassy polymer film of thickness s_0. (*b*) Solvent diffuses into polymer and forms swollen gel layer. The solvent-gel boundary s can move toward the solvent (swelling) in the early stages of dissolution. (*c*) Solvent continues to penetrate further into the glassy region. In the gel region, polymer molecules disentangle and diffuse into the solvent. The solvent-gel boundary retreats from the solvent.

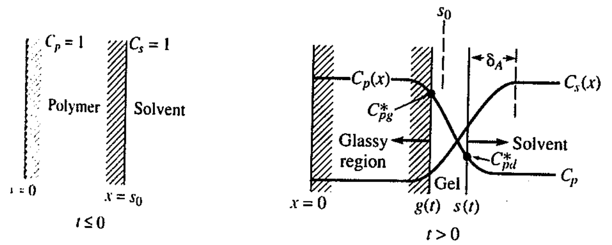

FIGURE 9-16
Concentration profiles (mole fractions) in the dissolving film.

to the resistance to mass transfer at that interface and contribute to a mass transfer coefficient k_d in a boundary condition on the development equations that we present shortly.

We establish a coordinate system x with origin $x = 0$ at the impermeable substrate. The initial polymer resist film thickness is $x = s_0$. The development solution-gel boundary, defined as the plane in which $C_p^* = C_{pd}^*$, moves in time as dissolution proceeds. At long times, this boundary is located at positions $s(t)$ which approach $x = 0$. At short times, depending on the solution thermodynamics, it is possible that swelling exceeds dissolution to the extent that $s(t)$ can be greater than s_0 (see Fig. 9-15), so that $ds/dt > 0$ for short times.

As the concentration C_s of *solvent* within the gel layer decreases (see Fig. 9-16), the diffusivity of solvent in polymer becomes exceedingly small. A region within the polymer film is reached where there is no significant penetration of solvent and no swelling of the polymer. The polymer in this region, and on to the boundary $x = 0$, is essentially in its original glassy state. Hence we define a glass-gel interface $g(t)$ by the critical polymer concentration $C_p = C_{pg}^*$. Of course, $g(t)$ eventually approaches $x = 0$ as dissolution becomes complete.

With these physical ideas in mind we can put together a diffusion model for the development process. We use the volume fraction of solvent within the resist film as the concentration variable, in general. We could, as well, use the volume fraction of polymer. Since the sum of the fractions must be unity, i.e.,

$$C_p + C_s = 1 \tag{9-26}$$

the choice seems to matter little. It is simply a matter of convenience that is sometimes dictated by whether certain physical properties are available in one set of units or the other. We follow the approach presented by Lee and Peppas [R9-27] for transient one-dimensional diffusion of solvent into and through a thin polymer film:

$$\frac{\partial C_s}{\partial t} = \frac{\partial}{\partial x}\left(\mathcal{D}_s \frac{\partial C_s}{\partial x}\right) \tag{9-27}$$

with initial condition

$$C_s = 0 \qquad \text{on } 0 \le x \le s_0 \text{ for } t \le 0 \tag{9-28}$$

Equation 9-27 is written for a fixed coordinate system with $x = 0$ at the solid substrate. Another approach to this analysis is given by Tu and Ouano [R9-28], who use a coordinate system fixed at the position s.

At the impermeable boundary $x = 0$ we have the condition

$$\frac{\partial C_s}{\partial x} = 0 \qquad \text{at } x = 0 \tag{9-29}$$

At the boundary $s(t)$ between the gel and the developing solution, the velocity of that boundary represents a balance between the rate at which solvent enters the resist (which would *swell* the film) and the rate at which polymer dissolves into the developer (which would *thin* the film). Thus we write

$$\mathcal{D}_s \frac{\partial C_s}{\partial x} - k_d C_{pd}^* = \frac{ds}{dt} \qquad \text{at } x = s(t) \tag{9-30}$$

The parameter k_d may depend upon the hydrodynamics of the dissolution process, and so is not strictly a polymer/solvent property. The dissolution process at the boundary $s(t)$ may be thought of as a chemical reaction with reaction products (in this case dissolved polymer) carried away by diffusion and convection into the developer. The concentration C_{pd}^* is the equilibrium polymer volume fraction at the gel-developer boundary.

The position of the gel–glassy polymer interface $g(t)$ is determined by a dynamic condition:

$$C_s \frac{dg}{dt} = -\mathcal{D}_s \frac{\partial C_s}{\partial x} \qquad \text{at } x = g(t) \tag{9-31}$$

In addition, the transition from the gel region to the glassy region must be defined thermodynamically. This is normally done by defining a *gel concentration* C_{sg}^* such that $g(t)$ is defined by

$$C_s = C_{sg}^* \qquad \text{at } x = g(t) \tag{9-32}$$

or

$$C_p = 1 - C_{sg}^* \equiv C_{pg}^* \tag{9-33}$$

The model presented here has three parameters related to the polymer-developer system: the concentrations C_{pd}^* and C_{pg}^* and the diffusion coefficient $\mathcal{D}_s$ of *solvent in polymer*. As presented, the diffusion coefficient is taken as a constant independent of concentration. (Tu and Ouano [R9-28] do not make this simplifying assumption.)

This model of development kinetics is mathematically complex, largely because the boundaries $s(t)$ and $g(t)$ move in time. A quasi–steady-state approximation is possible, however, in which it is assumed that diffusion is so rapid, in comparison to the velocities ds/dt and dg/dt, that at any time within the glassy region and the gel region the concentration profile has its steady-state character. For a one-dimensional "slab" geometry, this means that C_s is linear across each region.

With that assumption, Eqs. 9-31 and 9-30 reduce to the forms

$$(1 - C_{pg}^*)\frac{dg}{dt} = \frac{\mathcal{D}_s(C_{pd}^* - C_{pg}^*)}{s(t) - g(t)} \tag{9-34}$$

$$\frac{ds}{dt} = \frac{\mathcal{D}_s(C_{pg}^* - C_{pd}^*)}{s(t) - g(t)} - k_d C_{pd}^* \tag{9-35}$$

When Eq. 9-34 is subtracted from Eq. 9-35 we find

$$\frac{d(s-g)}{dt} = \left[\frac{\mathcal{D}_s(C_{pg}^* - C_{pd}^*)(2 - C_{pg}^*)}{(1 - C_{pg}^*)}\right]\frac{1}{s-g} - k_d C_{pd}^* \tag{9-36}$$

$$(s - g) = 0 \qquad \text{at } t = 0 \tag{9-37}$$

The solution for $(s - g)$, which is the thickness of the gel region, may be written in the form

$$-A\delta - AB \ln\left(1 - \frac{\delta}{B}\right) = \tau \tag{9-38}$$

where a dimensionless gel thickness is given by

$$\delta = \frac{s - g}{s_0} \tag{9-39}$$

and physical parameters are defined as

$$A = \frac{\mathcal{D}_s}{s_0 k_d C^*_{pd}} \tag{9-40}$$

and

$$B = \frac{\mathcal{D}_s (C^*_{pg} - C^*_{pd})(2 - C^*_{pg})}{s_0 k_d C^*_{pd}(1 - C^*_{pg})} \tag{9-41}$$

It is convenient to define a dimensionless time as

$$\tau = \frac{\mathcal{D}_s t}{s_0^2} \tag{9-42}$$

Once $\delta(\tau)$ is obtained, Eq. 9-34 or 9-35 will yield $g(t)$ and $s(t)$. Note, however, that Eq. 9-38 is not explicit in $\delta(\tau)$, so explicit solutions for s and g are not obtainable.

For short times, for which $\delta/B << 1$, an approximation to the logarithmic term in Eq. 9-38 yields the result

$$\delta = \left(\frac{2B}{A}\tau\right)^{1/2} \tag{9-43}$$

For short times the thickness δ of the gel region grows with the square root of time. For the longer term the behavior of δ follows from Eq. 9-38. If a new dimensionless time

$$\tau' = \frac{\tau}{AB} \tag{9-44}$$

is defined we can write Eq. 9-38 as

$$-\frac{\delta}{B} - \ln\left(1 - \frac{\delta}{B}\right) = \tau' \tag{9-45}$$

[Note that by rescaling the time variable to τ', Eq. 9-45 has only one parameter, B, upon which $\delta(\tau')$ depends.] Figure 9-17 shows $\delta(\tau', B)$. By plotting δ/B vs. τ', a single curve results for all B values. Clearly the parameter B plays an important role in controlling the rate of development. Some of the parameters in B (see Eq. 9-41) are available for specific polymer-solvent pairs. But k_d is not generally known. It must be obtained from the dissolution data. The model outlined here gives us a method for obtaining k_d.

Example 9-3.1 Determination of model parameters. We begin by writing Eq. 9-36 in dimensionless format, with the result

$$\frac{d\delta}{d\tau} = \frac{B}{A}\frac{1}{\delta} - \frac{1}{A} \tag{9-46}$$

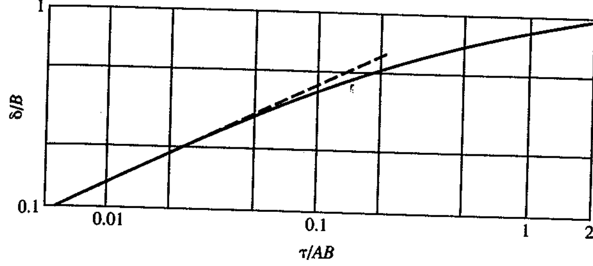

FIGURE 9-17
Gel region thickness as a function of time, according to Eq. 9-45.

We can see that δ approaches a maximum $(d\delta/d\tau = 0)$ at a value

$$\delta_{max} = B \tag{9-47}$$

Hence observation of the maximum gel layer thickness permits determination of B.

Using Eq. 9-45, we may find the time at which the maximum value of δ is reached by substituting B for δ, with the result

$$\tau'_{max} \to \infty \qquad \text{as } \delta \to B \tag{9-48}$$

We see, then, that δ_{max} is approached asymptotically at long times.

The slope of the short-time data, when plotted as δ vs. $\tau^{1/2}$, is found from Eq. 9-43. Hence the slope gives a value of B/A. Thus we can find A and B from δ_{max} and the initial slope of a plot of δ vs. $\tau^{1/2}$.

We use these results to examine some data on polymer film dissolution. The data, seen in Figure 9-18, are for the dissolution of PMMA (polymethyl methacrylate) in

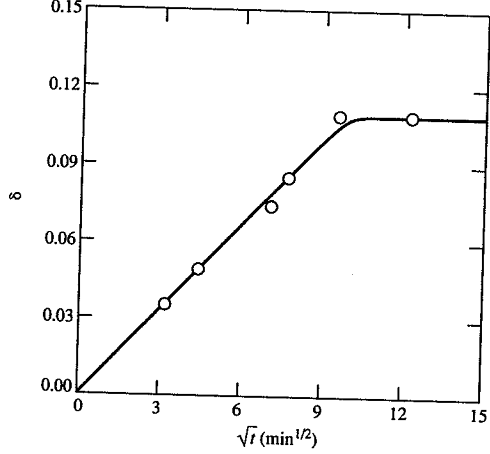

FIGURE 9-18
Normalized gel thickness data for Example 9-3.1.

methyl ethyl ketone (MEK) at 26°C [R9-10]. We see that δ attains a maximum at the value $\delta_{max} = 0.11$.

If the model outlined here is valid, then from Eq. 9-47 we find $B = 0.11$.

Values of C^*_{pg} and $\mathcal{D}_s$ are independently available and we use

$$C^*_{pg} = 0.74 \qquad \mathcal{D}_s = 5.2 \times 10^{-7}\ \text{cm}^2/\text{s} \tag{9-49}$$

The initial film thickness corresponds to

$$s_0 = 0.11\ \text{cm} \tag{9-50}$$

The data do indeed show a linear region when plotted against $t^{1/2}$, and from Figure 9-18 we find a slope of 0.011 $\text{min}^{-1/2} = 1.4 \times 10^{-3}\text{s}^{-1/2}$.

From Eq. 9-43 we write

$$\delta = \left(\frac{2B}{A}\frac{\mathcal{D}_s}{s_0^2}\right)^{1/2} t^{1/2} = 1.4 \times 10^{-3} t^{1/2} \tag{9-51}$$

Using $B = 0.11$ and $\mathcal{D}_s$ and s_0 given above, we find

$$A = 4.7 \tag{9-52}$$

From their definitions we find

$$\frac{A}{B} = \frac{1 - C^*_{pg}}{(C^*_{pg} - C^*_{pd})(2 - C^*_{pg})} = \frac{4.7}{0.11} = 43 \tag{9-53}$$

Using $C^*_{pg} = 0.74$ we find

$$C^*_{pd} \approx 0.74 \tag{9-54}$$

On physical grounds, in view of their definitions, we would expect C^*_{pd} to be much lower than C^*_{pg}. Their near equality (Eq. 9-54) follows from the fact that $A/B >> 1$. We now find k_d from the definition of A:

$$k_d = \frac{\mathcal{D}_s}{s_0 C^*_{pd} A} = 1.4 \times 10^{-6}\ \text{cm/s} \tag{9-55}$$

As a check on consistency of this model we examine the time at which δ reaches half its asymptotic value, i.e., the time $t_{1/2}$ at which $\delta/B = 0.5$. From Figure 9-17 we find

$$\frac{\delta}{B} = 0.5 \qquad \text{at } \frac{\tau}{AB} = 0.19 \tag{9-56}$$

Using the A and B values determined earlier we predict

$$\frac{t_{1/2}\mathcal{D}_s}{s_0^2} = 0.19AB = 9.8 \times 10^{-2} \tag{9-57}$$

or

$$t_{1/2} = 2290\ \text{s} \qquad \text{(predicted)} \tag{9-58}$$

From Figure 9-18 we find

$$t_{1/2} = 3380\ \text{s} \qquad \text{(measured)} \tag{9-59}$$

This example suggests that the major features of the kinetics of the early stage of development (the formation of the gel layer) are described qualitatively by the simple model outlined here. Unfortunately we know of no other data that show the characteristic features of Figure 9-17. Hence we are not able to provide a stronger argument in favor of this part of the model.

We turn now to the latter stages of dissolution. Equation 9-35 gives the desired $s(t)$ behavior. We nondimensionalize Eq. 9-35 to yield

$$\frac{d\sigma}{d\tau} = \frac{C^*_{pg} - C^*_{pd}}{\delta} - \frac{1}{A} \tag{9-60}$$

with

$$\sigma = \frac{s}{s_0} = 1 \qquad \text{at } \tau = 0 \tag{9-61}$$

As noted previously, δ becomes a constant ($\delta \approx B$) only asymptotically for $t \to \infty$. However, from Figure 9-17 we may approximate the end of the gel growth regime by

$$\tau_{max} \approx 2AB \tag{9-62}$$

If we set $\delta = B$ in Eq. 9-60, we find

$$\frac{d\sigma}{d\tau} = \frac{C^*_{pg} - C^*_{pd}}{B} - \frac{1}{A} \tag{9-63}$$

Using the definitions of A and B we may eliminate $C^*_{pg} - C^*_{pd}$ to find

$$\frac{d\sigma}{d\tau} = \frac{1}{A}\left[\frac{1 - C^*_{pg}}{2 - C^*_{pg}} - 1\right] \equiv -R' \tag{9-64}$$

subject to the initial condition

$$\sigma = 1 + B \qquad \text{at } \tau = 2AB \tag{9-65}$$

Here, R' is the *dimensionless* dissolution rate. The solution is

$$\sigma - (1 + B) = -R'(\tau - 2AB) \tag{9-66}$$

We define the dissolution time as the τ at which $\sigma = 0$, so we find

$$\tau_d = \frac{1 + B}{R'} + 2AB \tag{9-67}$$

For polymer-solvent pairs that exhibit a very small degree of swelling ($B << 1$), Eq. 9-67 simplifies to

$$\tau_d \approx \frac{1}{R'} = (2 - C^*_{pg})A \tag{9-68}$$

or, in terms of real time,

$$t_d = \frac{s_0(2 - C^*_{pg})}{k_d C^*_{pd}} \tag{9-69}$$

This result implies several things. First, we note that the diffusion coefficient $\mathcal{D}_s$ does not appear in Eq. 9-69. This follows from the assumption, in passing from Eq. 9-67 to Eq. 9-68, that swelling plays no significant role ($B << 1$). In this model, dissolution is dominated by the removal of polymer molecules from the interface at $s(t)$. Hence the coefficients k_d and C^*_{pd} play the central role. We note also that the development

time *appears* (Eq. 9-69) to be linear in resist thickness s_0. We must recall, however, that the fraction of absorbed energy, in the case of *e*-beam radiation, is dependent upon resist thickness. As a consequence, the molecular weight of the resist following irradiation, and so the physical properties such as k_d and C^*_{pd}, could depend upon s_0. This would actually produce a nonlinear dependence of t_d on s_0.

An example of data to which this model applies is presented in Figure 9-19 [R9-35]. We see that there is no evidence of significant swelling ($B << 1$) and that s falls linearly with time, as Eq. 9-66 predicts. Hence the dissolution rate R is constant, and it is given in terms of the development time t_d as

$$R = \frac{s_0}{t_d} \tag{9-70}$$

In Figure 9-20 we show R as a function of molecular weight. The data are described approximately by (see Eq. 9-13)

$$R = 7.6 \times 10^8 M_n^{-1.7} \text{ (Å/min)} \tag{9-71}$$

The data of Figures 9-19 and 9-20 were obtained under quiescent conditions in the developing bath. It is interesting to raise the question of whether the development time could be reduced by agitation of the bath. The key to answering the question lies in examination of Eq. 9-69. We must know more about the parameter k_d. If it represents a convective mass transfer coefficient, for example, then we should be able to promote development through agitation of the bath. A study of the literature suggests, however,

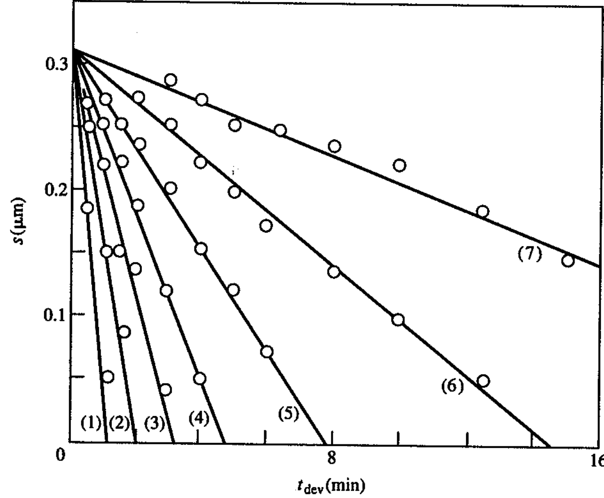

FIGURE 9-19
Dissolution of an acrylic resist at various levels of molecular weight: (1) 1800; (2) 2300; (3) 2700; (4) 3400; (5) 4600; (6) 6600; (7) 13,000.

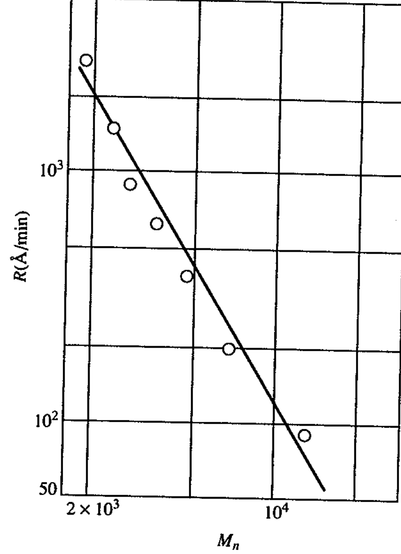

FIGURE 9-20
Data of Figure 9-19 converted to rate of dissolution as a function of molecular weight.

that k_d is related to the physical process through which an entangled polymer molecule at the surface $s(t)$ becomes disentangled. The kinetics of disentanglement is believed to be the rate-controlling step, rather than the convection and diffusion of the polymer molecule away from the surface.

Evidence for this lies in examination of the temperature dependence of the dissolution rate. Figure 9-21 shows data [R9-31] for dissolution rate vs. temperature, in a form that permits calculation of an activation energy. We write

$$R = R_0 \exp\left(\frac{-E_a}{R_G T}\right) \tag{9-72}$$

where R_G is the gas constant [1.987 cal/g · mol · K]. These data correspond to an activation energy of 25 kcal/mol. This is more than twice the activation energy associated with diffusion, and it is suggestive of the idea that k_d is associated with a process independent of diffusion and convection external to the surface at $s(t)$.

9-4 RESIST PROFILE DEVELOPMENT

In the chain scission model described earlier (Eq. 9-8) the dose of radiation D refers to radiation energy *absorbed* at some region interior to the photoresist layer. Thus D is really a function of spatial position; we refer to it hereafter as the function $E(x, y)$, where y is the coordinate normal to the plane of the layer. The spatial distribution of absorbed radiation depends upon the incident radiation, which itself could be some

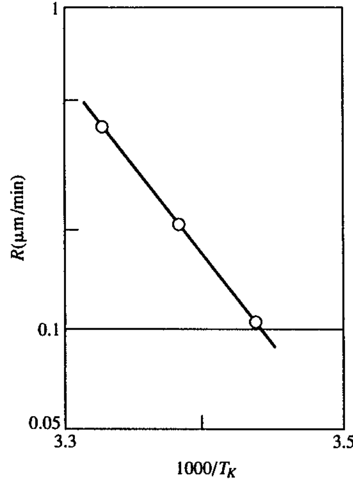

FIGURE 9-21
Dissolution rate for PMMA in MEK as a function of temperature.

function $E_0(x)$, and on the absorbing and scattering characteristics of the resist, as well as on reflection from the substrate.†

We assume first that the radiation physics is sufficiently understood that the function $E(x, y)$ is available under a given set of conditions. We wish to connect $E(x, y)$ with the dissolution rate R. Since Eq. 9-8 is available, we need first to connect R to M_n. This is usually done [R9-32] through the empirical relationship (see Eq. 9-13)

$$R(x, y) = R_0 + \beta(M_n)^{-\alpha} \tag{9-73}$$

Upon combining Eqs. 9-73 and 9-8 we find

$$R(x, y) = R_0 + \beta\left[\frac{1}{M_n^0} + \frac{GE(x, y)}{100N_A}\right]^{\alpha} \tag{9-74}$$

Thus we see that contours of uniform radiation absorption, i.e., lines of $E(x, y) =$ constant, will be transformed into contours of uniform removal rate. If dissolution is controlled by the function $R(M_n^*)$, rather than by convection and diffusion external to the gel-solution boundary, then we expect the development contours (such as those shown in Figure 9-5) to coincide with contours of $R(x, y) =$ constant.

Various computational algorithms have been developed for predicting resist profiles. References are provided at the end of this chapter.

†Note that we take the incident radiation to correspond to a one-dimensional (line) source. As a result we consider only two-dimensional profiles here.

9-5 SPIN COATING OF RESIST

To this point we have assumed that we begin with a thin uniform layer of resist on the wafer substrate. Now we examine the fluid dynamics of the process by which the resist layer is created. The most common procedure is spin coating.

The most widely used positive resists are coated from polymer solutions. A small quantity of solution is dispensed onto the wafer center, and the wafer is spun at an accelerating rotational speed to distribute the solution across the wafer. The wafer is then spun at constant speed, typically in the neighborhood of several thousand revolutions per minute, to produce a very thin uniform film.

There are a number of questions to be raised in considering the spin coating process:

1. How does coating thickness depend upon spin speed, fluid properties, and spin duration?
2. How uniform is coating thickness across the radius of the wafer?
3. To what degree is coating behavior affected by the non-newtonian properties common to many polymer solutions?
4. To what degree does solvent evaporation affect coating behavior?

We begin to address these questions by considering a relatively simple fluid dynamic analysis.

9-5.1 Spin Coating of a Nonvolatile Newtonian Liquid

We assume axisymmetric laminar flow under isothermal conditions. Inertial effects are assumed to be much less than viscous effects, an assumption that seems quite reasonable for fairly viscous liquids in very thin films. We assume a uniform pressure distribution within the film. Then the radial component of the Navier-Stokes equations is simply (see Eq. 3-73)

$$\mu\frac{\partial^2 v_r}{\partial z^2} = -\rho\omega^2 r \tag{9-75}$$

where μ and ρ are the liquid viscosity and density. Figure 9-22 defines the coordinate system.

The local film thickness $h(r, t)$ is determined by a material balance, which leads to (see Eq. 3-81)

$$\frac{\partial h}{\partial t} = -\frac{1}{r}\frac{\partial}{\partial r}(rq) \tag{9-76}$$

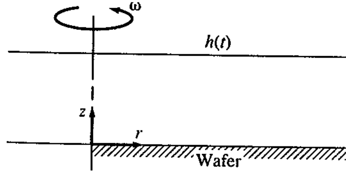

FIGURE 9-22
Coordinate system for analysis of spin coating.

where q is the volumetric flowrate per unit length of circumference, defined by

$$q = \int_0^h v_r \, dz \tag{9-77}$$

Boundary conditions assume no slip at the wafer surface:

$$v_r = 0 \qquad \text{at } z = 0 \tag{9-78}$$

and no shear stress at the free surface:

$$\frac{\partial v_r}{\partial z} = 0 \qquad \text{at } z = h(r, t) \tag{9-79}$$

These equations are easily solved to yield

$$v_r = \frac{\rho\omega^2 r}{2\mu} h^2(t) \left\{ 1 - \left[1 - \frac{z}{h(t)} \right]^2 \right\} \tag{9-80}$$

and

$$q = \frac{\rho\omega^2 r}{3\mu} h^3(t) \tag{9-81}$$

This gives a differential equation for $h(r, t)$ in the form

$$\frac{\partial h}{\partial t} + \frac{\rho\omega^2}{3\mu} \frac{1}{r} \frac{\partial}{\partial r}(r^2 h^3) = 0 \tag{9-82}$$

For the case of an initially uniform film of thickness h_0, that is, for

$$h = h_0 \qquad \text{at } t = 0 \text{ for all } r \tag{9-83}$$

the solution is easily found to be

$$\frac{h}{h_0} = \left(1 + \frac{4\rho\omega^2}{3\mu} h_0^2 t \right)^{-1/2} \tag{9-84}$$

Two points are immediately apparent. One is that if the film is initially uniform with respect to r [i.e., $h(r) = h_0 =$ constant], then it remains uniform for all subsequent time. The second point is that for very thin films, by which we mean for $h << h_0$, the film thickness decreases like

$$h = \left(\frac{3\mu}{4\rho} \right)^{1/2} \omega^{-1} t^{-1/2} \tag{9-85}$$

One of the most interesting elements of this result is that for long times, the film thickness is independent of its initial value.

Figure 9-23 presents data for spin coating of various nonvolatile newtonian fluids. The agreement with the prediction of Eq. 9-85 is quite good; the data show coating thicknesses about 10% above the theoretical values, and this deviation is within the expected error for the technique used.

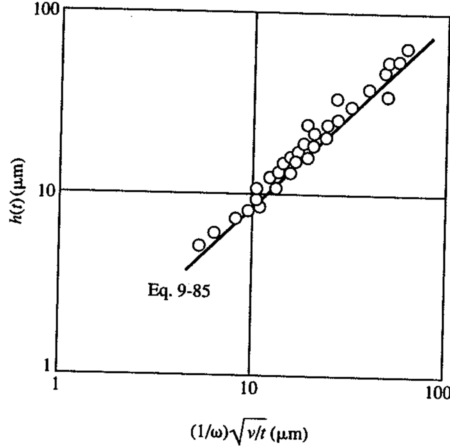

FIGURE 9-23
Data for spin coating of silicon oils. Viscosities range from 10 to 10^4 Pa·s.

9-5.2 Planarization

Resist is often applied after some topographical features have already been etched into a layer on the wafer surface. Coating over a nonplanar surface will produce a film of resist which is not planar but reflects to some degree the underlying surface topography. The degree of nonuniformity, i.e., the deviation from planarization, and the possibility of control of this deviation are the issues of concern in this section.

We begin with a review of the work of White [R9-48]. Figure 9-24 shows a coating over an isolated line feature. If H_1 is the amplitude of the initial (uncoated) step and H_2 is the amplitude over that step above the level of the subsequent film, then we may define the ratio H_2/H_1 as a measure of the effect of the feature on the subsequent coating. We would expect that H_2/H_1 would be a function of the film thickness far from the feature H_∞. Figure 9-25 shows data typical of this effect for several resists. Small values of the ratio H_2/H_1 correspond to a high degree of planarization. One would like to achieve planarization with a minimal amount of coating, H_∞. Alternatively, a large (negative) slope of data as in Figure 9-25 corresponds to a resist which achieves good planarization with minimal incremental coverage. The magnitude of the slope is defined as the *planarization constant*.

The planarization constant depends upon the viscosity of the resist, as Figure 9-26 suggests. We see that the lower viscosity resists have a larger (hence better)

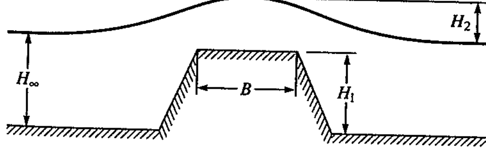

FIGURE 9-24
Resist profile spun over an isolated line feature.

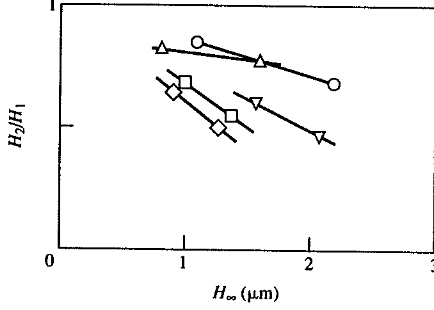

FIGURE 9-25
Degree of planarization as a function of film thickness. $B = 20\ \mu m$; $H_1 = 1\ \mu m$.

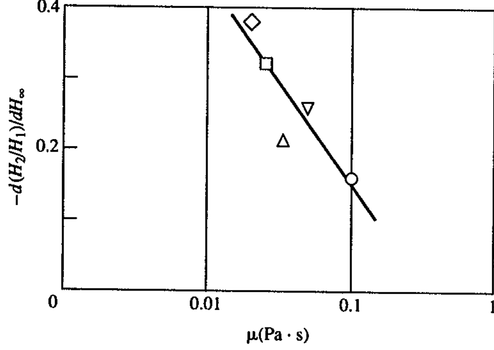

FIGURE 9-26
Planarization constant as a function of resist viscosity.

planarization constant. The geometry of the feature being covered is also a factor that affects planarization. Figure 9-27 shows H_2/H_1 values as a function of the breadth B of a feature. Two resists that differ primarily in viscosity show significantly different dependencies on feature geometry.

The data just described are for lines that are oriented *radially*, i.e., their long axis (about 500 μm in all cases) points toward the wafer center. In a subsequent study, White and Miszkowski [R9-47] compared the effects of feature orientation on planarization. Figure 9-28 exhibits orientation effects for a specific resist. The notation $\perp$ and $\|$ refers to lines oriented with their axis either perpendicular or parallel to a wafer radius, respectively. The authors do not state the thickness H_∞ corresponding to these data but do indicate that resist is spun for 30 s. We might assume, then, that the 4K and 6K pairs represent different values of H_∞, corresponding to spinning at 4000 and 6000 rpm, and that the 6K data have the smaller values of H_∞. The relative position of the 4K and 6K curves is then seen to be consistent with the data of Figure 9-25.

Orientation effects are modest but visible. Planarization is better for the parallel orientation, and as seen earlier, planarization is difficult to achieve for large features. One would expect that the function H_2/H_1 would become independent of orientation

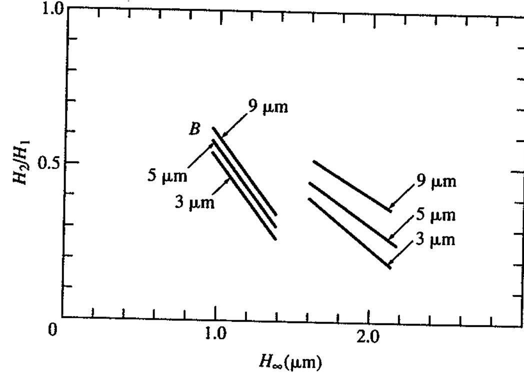

FIGURE 9-27
Dependence of degree of planarization on breadth of a feature.

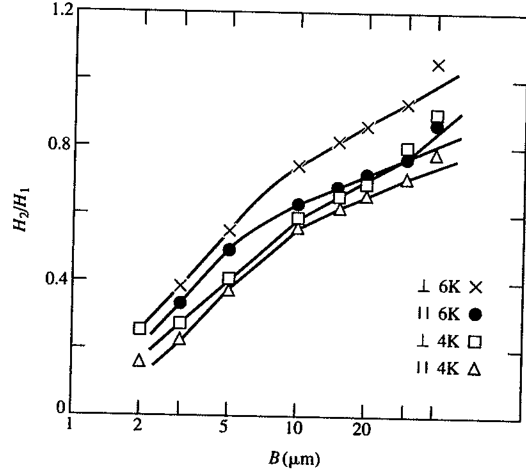

FIGURE 9-28
Dependence of planarization constant on orientation of a feature.

when B becomes large in comparison to H_1. This trend would be more evident if a logarithmic scale were used for H_2/H_1, but it appears to be borne out by the data presented.

All of the foregoing results are for isolated features. White and Miszkowski also present results for a 10- by 10-μm grating with a nominal 1-μm step height, with the 500-μm axis (length) oriented parallel to the flow. As expected, since the breadth and

the distance between steps are each 10 times the height, the degree of planarization is poor, as Figure 9-29 shows. Furthermore, and also as expected, orientation does not have a larger effect on a grating of these dimensions.

One must keep in mind that a fluid dynamic interpretation of the kinds of results presented here is made complicated by the fact that the resist is losing solvent, and hence becoming very viscous, during the spinning process. Thus the behavior exhibited by a particular resist depends not only on its viscosity but also on its evaporation rate and the concentration dependence of its viscosity. Relevant studies of these effects are cited at the end of this chapter.

An additional complication lies in the fact that after a resist is coated upon some topography, the wafer may undergo heat treatment to remove residual solvent, or to cure the film. Polymer flow can occur during this phase, and this subsequent flow could significantly alter the degree of planarization. White [R9-46] shows an example of this phenomenon for a polyimide resist film (see Fig. 9-30). Isolated features with breadths in the range of 3–50 μm were coated. It is assumed that these were all 1-μm step heights, and the subsequent film would be expected to show amplitudes of about

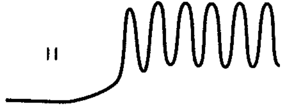

FIGURE 9-29
Coating profiles over a grating, for parallel and perpendicular orientations. (The horizontal axis is not to scale.)

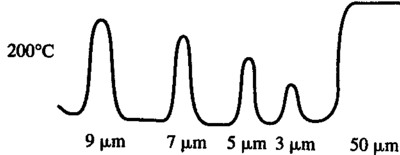

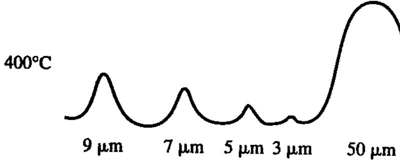

FIGURE 9-30
Effect of curing temperature on coating profiles.

1 μm except for the smallest features. The upper trace in Figure 9-30 may be taken as nearly the original coated profile, since little flow is to be expected in the polymer film at this temperature. A dramatic reduction in amplitudes, i.e., significantly improved planarization, occurs at 400°C.

It is worthwhile to inquire into the mechanism of postspin planarization during a curing operation. We ask the following questions:

1. What forces act upon the film, capable of causing planarization?
2. What are the relative magnitudes of these forces and of the flowrates that might be expected to arise from these forces?

After some thought, it would appear that only two forces are available to induce planarization on a static wafer (see Fig. 9-31). One is gravitational. Assuming that the wafer is horizontal, then hydrostatic pressure of the order of

$$P_g = \rho g H_2 \tag{9-86}$$

would be available to induce leveling. Using order of magnitude estimates of $\rho = 1$ and $g = 980$ (cgs units) and considering a 1-μm height (10^{-4} cm), we find $P_g = O(0.1)$ dyn/cm^2.

A second force arises from interfacial tension, and the curvature of the interface. The pressure associated with this phenomenon is of the order of

$$P_s = \frac{\sigma}{R_c} \tag{9-87}$$

where R_c is the mean radius of curvature and σ is the interfacial tension. Typical values of σ for a polymer melt would be $\sigma = 20$ dyn/cm. For a small feature we may use the amplitude H_2 as an estimate for R_c, and we find, for $H_2 = 1$ μm,

$$P_s = \frac{20}{10^{-4}} = 2 \times 10^5 \text{ dyn/cm}^2 \tag{9-88}$$

It is clear, then, that surface tension dominates gravitational effects, but this still does not indicate the magnitude of flow to be expected from such a pressure. This may be estimated by using an analogy to a squeezing flow (see Fig. 9-32). We inquire into the rate of thinning of a liquid film being squeezed between two surfaces, under a pressure comparable to P_s. The squeezing flow problem may be solved (see Prob. 9-17), and

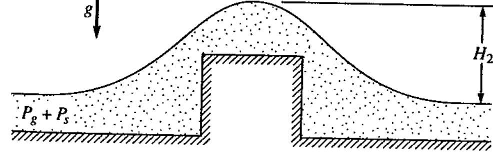

FIGURE 9-31
Leveling is driven by gravitational and surface tension forces.

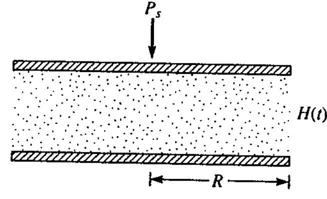

FIGURE 9-32
A squeezing flow analog to leveling under surface tension.

the film thickness, as a function of time, is found to be

$$\left(\frac{H_0}{H}\right)^2 = 1 + \frac{16P_s H_0^2 t}{3R^2\mu} \tag{9-89}$$

We may define a half-time as $t = t_{1/2}$ when $H = H_0/2$. Then it follows that

$$t_{1/2} = \frac{9R^2\mu}{16H_0^2 P_s} \tag{9-90}$$

We use our estimate of $P_s = 2 \times 10^5$ dyn/cm^2, take R/H_0 =O(1), and estimate μ for a molten polymer at 400°C to be 100 poise. Then we find

$$t_{1/2} = 2.8 \times 10^{-4} \text{ s} \tag{9-91}$$

This is a very short time, indicating that considerable planarization could be expected to occur under the mechanism of surface tension–driven flow. Even if the feature were an order of magnitude larger (thus reducing P_s), and if the viscosity were an order of magnitude larger, and if the feature were 10 times as broad as its height ($R/H_0 = 10$), there would still be time for a significant degree of planarization to occur under this mechanism.

We note that this model is consistent with the observation that very little planarization occurs over a 50-μm feature (R is very big) while small features "flow out" almost completely. Although this simple model does not have much quantitative basis for its application, it does suggest that the surface tension of the molten polymer is a key parameter to be explored in developing resists with improved planarization properties. Unfortunately, there is not much latitude in surface tension values in molten polymers, but one should exploit whatever latitude there is.

PROBLEMS

9-1. Exposure requirement for a PMMA resist. A PMMA resist with $M_n^0 = 167{,}000$ is exposed to ^{60}Co γ-radiation with a flux of 10 Mrad/s. Assume the properties of the resist are described by the data in Figure P9-1. What exposure time is required to reduce M_n to 50,000?

9-2. Determination of radiation chemical yield. Using the data in Figure 9-3, calculate the radiation chemical yield G, in units of chain scissions per 100 eV. Assume that γ-radiation is completely absorbed by PMMA.

9-3. Sensitivity of PMMA to γ-radiation. Parsonage, Peppas, and Lee [R9-10] present the data tabulated below for a PMMA polymer with an initial number average molecular weight of 225,000. Samples were irradiated with γ-rays in a ^{60}Co unit under nitrogen, with a *dose rate* of 2864 rad/min. (Note that 1 Mrad corresponds to 6.25×10^{19} eV/g.)

Dose, Mrad	M_n
0	225,000
2.1	175,000
4.1	93,000
6.2	60,000

Find the G for this polymer. (The authors of this reference give a value of 1.3 scissions/100 eV.)

9-4. G values for PMMA resists. Hatzakis et al. [R9-5] present the following data on 1-μm-thick PMMA resist films under 25-keV e-beam radiation. Give the G values of each polymer.

PMMA I

Dose, μC/cm^2	0	8	12	16	20	24	32	36	40
$M_n \times 10^{-3}$	49.5	27.8	26	19.7	16.3	14.5	12.1	10.8	10.6

PMMA II

Dose, μC/cm^2	0	8	16	32	36
$M_n \times 10^{-3}$	20.3	16.3	12	9.6	9.4

9-5. G Values for PMMA. Shultz et al. [R9-7] present data for e-beam irradiated PMMA. The authors state that the energy absorbed was calculated according to the conversion of 1.0 megarep = 5.24×10^{19} eV/g. Note that the *weight* average molecular weight M_w is measured. Assume that $M_w = 2M_n$. Give the G value in units of chain scissions/100 eV.

D, Mreps	0	3.3	5.5	6.6	11	22
$M_w \times 10^{-6}$	3.2	0.41	0.24	0.155	0.131	0.054

9-6. G Value for polyisobutylene. Chapiro [R9-8, p. 499] presents data on chain scission under gamma irradiation for a rubbery polymer, polyisobutylene (PIB). Find the G value for PIB. Use the conversion 1 Mroentgen = 5.5×10^{19} eV/g.

D, Mroentgen	0	1.4	3.8	6.5	11.7	15.6	30.3
$M_n \times 10^{-3}$	480	280	190	110	55	52	22

9-7. Absorption efficiency of e-beam radiation in PMMA. Kyser and Murata [R9-6] give calculated values of e-beam energy deposition in PMMA films, as shown in Figure P9-2. In all cases the PMMA film was on an aluminum substrate. How compatible are these calculations with those of Hatzakis et al. [R9-5]? Answer by plotting the incident energy at which the film absorbs one-third of the incident radiation, as a function of film thickness. Compare the results obtained from Figure P9-2 to those from Figure 9-2.

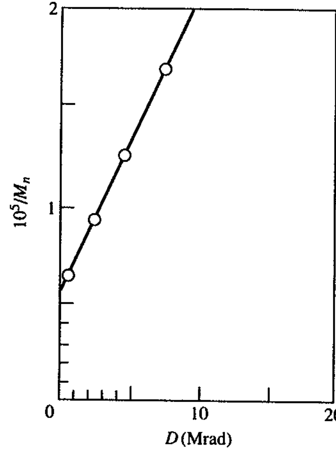

FIGURE P9-1
Inverse molecular weight as a function of dose for PMMA.

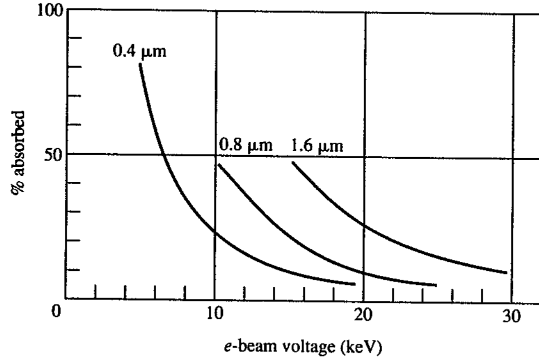

FIGURE P9-2
Absorption of *e*-beam energy by PMMA films on aluminum.

9-8. Effect of dose on solubility rate. Hatzakis et al. [R9-5] present the data shown in Figure P9-3 for development of a PMMA positive resist using MIBK developer. These authors point out that an important measure of positive resist performance is the increase of solubility rate R with exposure dose. (*a*) Determine $R(D)$ from these data, and plot $[R(D) - R(0)]/R(0)$ vs D. (*b*) Give the exposure dose required to increase R by an order of magnitude over the unexposed rate $R(0)$.

9-9. Effect of molecular weight on solubility rate. A PMMA positive resist, with an initial number average molecular weight of 10^5, has a G value of 0.75 chain scissions/100 eV and a solubility rate in MIBK at 25°C of 500 Å/min. If the solubility rate vs. molecular weight relationship is given by (see Eq. 9-73)

$$R = R_0 + 1.25 \times 10^9 M_n^{-1.4} \text{ (Å/min)} \quad \text{(P9-1)}$$

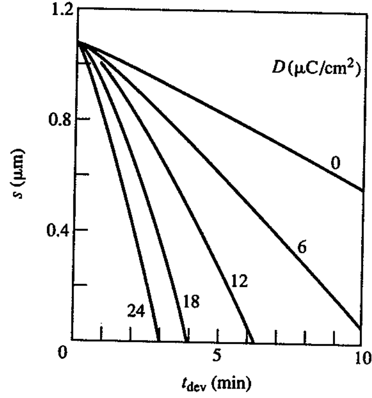

FIGURE P9-3
Development of PMMA resists in MIBK. Parameter is dose of 15-keV radiation.

give the dose of *e*-beam radiation, in μC/cm², required to yield a solubility rate of 4000 Å/min. Assume 15-keV electrons are used on a 1-μm resist film.

9-10. Development time vs. dose for PMMA. Plot development time (defined for the purpose of this problem as the time in minutes to dissolve a 0.5-μm film of resist) as a function of *e*-beam dose (in μC/cm²) for a resist with the following properties (see Eq. 9-73): $R_0 = 84$ Å/min; $\beta = 3.14 \times 10^8$ Å/min; $\alpha = 1.5$. The resist is PMMA with $M_n^0 = 2 \times 10^5$ and $G = 0.75$. Assume 20-keV electrons are used. Plot the "contrast function" $\Gamma(D)$ where

$$\Gamma \equiv 1 - \frac{R(0)}{R(D)} \quad \text{(P9-2)}$$

9-11. Mechanism of dissolution. Tu and Ouano [R9-28] infer that the dissolution of polystyrene (PS) by methyl ethyl ketone (MEK) is controlled by the kinetics of disentanglement of PS molecules from the gel-solution interface. An alternative hypothesis is that dissolution is controlled by diffusion of free polymer molecules across a convective boundary layer that separates the gel interface from the polymer-free solvent. If the latter were true, we would expect to find that the dissolution rate R would be given by

$$R \approx \frac{\mathcal{D}_p C^*_{pd}}{\delta} \quad \text{(P9-3)}$$

where $\mathcal{D}_p$ is the diffusivity of polymer in solvent and δ is the boundary layer thickness. Assume that δ is fixed by the conditions of development, and test Eq. P9-3 against the following observations:

$M_w \times 10^{-5}$	C^*_{pd}	X, (Å/min)
1.0	0.27	1.7×10^9
3.0	0.09	1.2×10^6
5.0	0.054	5.2×10^4
7.0	0.038	6.6×10^3
10.0	0.027	2.6×10^2

The diffusivity of polymer in solvent is

$$\mathcal{D}_p = 5.5 \times 10^{-4} M_w^{-0.56} \text{ cm}^2/\text{s} \tag{P9-4}$$

9-12. Effect of developer dilution on development time. The data in Figure P9-4 show the effect of developer strength on the rate of dissolution of a novolak resist. The developer is a commercial Shipley AZ (aqueous alkaline) developer with a pH (undiluted) of 12.9. The parameter on each curve is the volume ratio of developer to water. Plot development time against the ratio of AZ developer to water. Suppose the developer became progressively diluted by rinsewater over some period of time. What percentage change in concentration could be tolerated in an initial 1:1 developer solution if a 10% change in development time were tolerable?

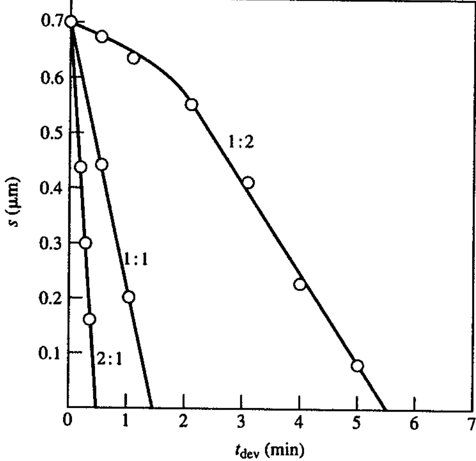

FIGURE P9-4
Effect of dilution of developer on development time.

9-13. The depth-dose function for e-beam absorption. Electron beam radiation is absorbed by a solid to a degree that depends upon the depth of penetration. The so-called depth-dose function may be calculated from

$$E_a(z) = \frac{D}{q}\frac{E_0}{R_G}\lambda(f) \tag{P9-5}$$

where the (empirical) function $\lambda(f)$ is given by Greenleigh [R9-35] as

$$\lambda(f) = 0.74 + 4.7f - 8.9f^2 + 3.5f^3 \tag{P9-6}$$

f is a normalized depth defined by

$$f = \frac{z}{R_G} \tag{P9-7}$$

where R_G is the so-called Gruen range of the solid. For PMMA

$$R_G = 3.8 \times 10^{-6} E_0^{1.75} \tag{P9-8}$$

with R_G in μm and E_0 in keV. For PMMA irradiated with a dose $D = 100$ μC/cm^2, plot the absorbed energy density (eV/cm^3) vs. depth z(μm) for accelerating voltages E_o of 5, 10, and 20 keV.

9-14. The fraction of absorbed energy from e-beam radiation. Define the average of the energy absorbed as

$$\overline{E}_a = \frac{1}{Z}\int_0^Z E_a(z)\,dz \tag{P9-9}$$

where $E_a(z)$ is the depth function given in Eq. P9-5. Show that

$$\frac{\overline{E}_a}{E_0} = \frac{0.74}{\mathbf{R}} + \frac{2.35}{\mathbf{R}^2} - \frac{3.0}{\mathbf{R}^3} + \frac{0.9}{\mathbf{R}^4} \tag{P9-10}$$

where

$$\mathbf{R} = \frac{R_G}{Z} \tag{P9-11}$$

Plot $\overline{E}_a/E_0$ against E_0 for PMMA films of thickness 0.5 and 1 μm.

9-15. Spin coating of a low–vapor pressure solution. Equation 9-84 may be written in a dimensionless format as

$$H = (1+\tau)^{-1/2} \tag{P9-12}$$

where

$$H = \frac{h}{h_0} \tag{P9-13}$$

and

$$\tau = \frac{4\rho\omega^2 h_0^2}{3\mu}t \tag{P9-14}$$

Jenekhe [R9-45] presents the data shown in Figure P9-5 for spin coating of two polymer solutions (polyvinyl acetate and polyamic acid) in low–vapor pressure (< 1.3 Pa at 20°C) solvents. For each solution the mass fraction of solids was approximately 20%. The data shown use for h the "dry-film" thickness subsequent to "baking" the wet film in an oven. The wet-film thickness was used for h_0. Test the following hypothesis: the solution spins

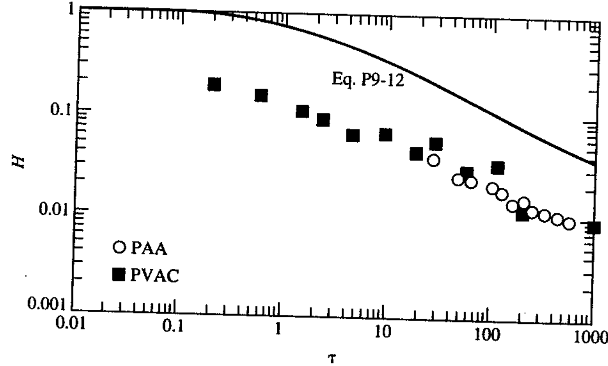

FIGURE P9-5
Spin coating data for Prob. 9-15. H is the dimensionless *dry* film thickness.

out to a uniform "wet" film, according to Eq. P9-12, in such a short time that there is no significant solvent loss. The observed dry film then follows upon baking the solvent out of the wet film, leaving behind the solids content only.

9-16. Spin coating of two resist solutions. Examine the spin coating data in a Figure P9-6 [R9-51]. Fluid I is a 28-cP viscosity Hunt Waycoat type IV photoresist with a solids fraction of 0.091. Fluid II is a 2040-cP Hitachi Chemical PIQ polyimide with a solids fraction of 0.11. Test Eq. P9-12 (and read Prob. 9-15 regarding evaporation) for each fluid. Speculate on the failure of fluid II to follow Eq. P9-12.

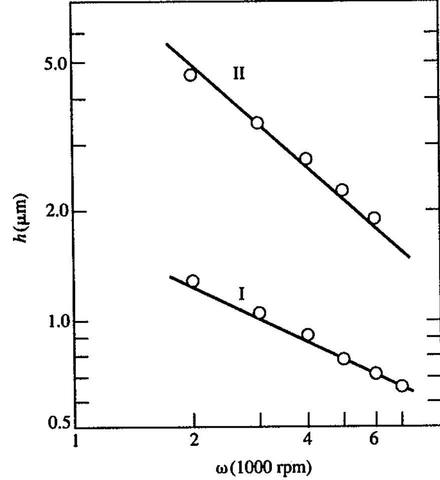

FIGURE P9-6
Spin coating data for Prob. 9-16.

9-17. A model of leveling. With reference to Figure 9-32, derive an expression for the squeezing of a film of viscous liquid between two plane parallel surfaces. Do two cases, corresponding to two different assumptions about the physics at the upper surface. In one case assume *no slip* of the fluid at that surface (as well as at the lower surface) and in the other case assume that there is *no shear stress* at the upper surface (while maintaining the no-slip assumption at the lower surface). What boundary conditions does Eq. 9-89 correspond to? Which of your two models is more realistic for the case of leveling?

REFERENCES

General references providing a broad background for much of this chapter

9-1. Thompson, L. G., C. G. Willson, and M. J. Bowden, eds., *Introduction to Microlithography*, ACS Symp. Ser. **219**, ACS, Washington, D.C., 1983.
9-2. Hatzakis, M., "Materials and Processes for Microstructure Fabrication," *IBM J. Res. Develop.*, **32**, 441 (1988).
9-3. Oberai, A. S., "Lithography—Challenges of the Future," *Solid State Technol.*, **30**(9), 123 (1987).
9-4. Stinson, S. C., "Electronics Industry Opens Frontiers for Photoresist Chemistry," *C&EN*, **23**, Sept. 26, 1983.

Radiation physics of polymer resists

9-5. Hatzakis, M., Ch. H Ting, and N. Viswanathan, "Fundamental Aspects of Electron Beam Exposure of Polymeric Resist System," *Proc. 6th Int. Conf. Electron and Ion Beam Sci. and Technol.*, Electrochemical Society, Princeton, N.J., 1974, p. 542.
9-6. Kyser, D., and K. Murata, "Monte Carlo Simulation of Electron Beam Scattering and Energy Loss in Thin Films on Thick Substrates," *Proc. 6th Int. Conf. Electron and Ion Beam Sci. and Technol.*, Electrochemical Society, Princeton, N.J., 1974, p. 205.

Early studies of effects of radiation on polymers

9-7. Shultz, A. R., P. Roth, and G. Rathmann, "Light Scattering and Viscosity Study of Electron-Irradiated Polystyrene and Polymethacrylates," *J. Polymer Sci.*, **22**, 495 (1956).
9-8. Chapiro, A., *Radiation Chemistry of Polymeric Systems*, Interscience, New York, 1962.

Recent fundamental research

9-9. Parsonage, E. E., and N. A. Peppas, "Properties of Positive Resists. I. Irradiation-Induced Degradation and Sensitivity of Certain Methyl Methacrylate Copolymers," *Brit. Polymer J.*, **19**, 469 (1987).
9-10. Parsonage, E. E., N. A. Peppas, and P. I. Lee, "Properties of Positive Resists. II. Dissolution Characteristics of Irradiated Poly(methyl methacrylate) and Poly(methyl methacrylate-co-maleic anhydride)," *J. Vac. Sci. Technol.*, **B5**, 538 (1987).

Sensitivity and contrast of resists

9-11. Feit, E. D., and L. E. Stillwagon, "Electron-Beam Lithography of Chlorinated Polystyrenes with Narrow Molecular Weight Distributions," *Polymer Engg. Sci.*, **20**, 1058 (1980).
9-12. Turner, S. R., R. A. Arcus, C. G. Houle, and W. R. Schleigh, "High-T_g Base-Soluble Copolymers as Novolac Replacements for Positive Photoresists," *Polymer Engg. Sci.*, **26**, 1096 (1986).
9-13. Gozdz, A. S., H. G. Craighead, and M. J. Bowden, "Poly(alkenylsilane Sulfone)s as Positive Electron Beam Resists for Two-Layer Systems," *Polymer Engg. Sci.*, **26**, 1123 (1986). See also Bowden, M. J., L. F. Thompson, S. R. Fahrenholtz, and E. M. Doerries, "A Sensitive Novolac-Based Positive Electron Resist," *J. Electrochem. Soc.*, **128**, 1304 (1981). This is the source of data for Prob. 9-12.
9-14. Ficke, H., E. W. Merrill, and N. Vasa, "Molten Poly(Methyl Methacrylate) under Electron Irradiation: Studies of Depropagation and Chain Scission," *Polymer Engg. Sci.*, **20**, 1236 (1980).
9-15. Liu, H.-Y., M. P. de Grandpre, and W. E. Feely, "Characterization of a High-Resolution Novolak-Based Negative Electron-Beam Resist with 4 $\mu C/cm^2$ Sensitivity," *J. Vac. Sci. Technol.*, **B6**, 379 (1988).
9-16. Itoh, T., Y. Yamashita, R. Kawazu, K. Kawamura, S. Ohno, T. Asano, K. Kobayashi, and G. Nagamatsu, "A Negative Resist, LMR (Low Molecular Weight Resist), for Deep UV Lithography," *Polymer Engg. Sci.*, **26**, 1105 (1986).
9-17. Novembre, A., L. Masakowski, and M. Hartney, "Optimal Developer Selection for Negative Acting Resists," *Polymer Engg. Sci.*, **26**, 1158 (1988).
9-18. Jagt, J. C., and A. Sevriens, "Electron Sensitive Negative Resists of Vinylaromatic Polymers," *Polymer Engg. Sci.*, **20**, 1082 (1980).
9-19. Shiraishi, H., Y. Taniguchi, S. Horigome, and S. Nonogaki, "Iodinated Polystyrene: An Ion-Millable Negative Resist," *Polymer Engg. Sci.*, **20**, 1054 (1980).
9-20. Thompson, L. F., E. D. Feit, and R. D. Heidenreich, "Lithography and Radiation Chemistry of Epoxy Containing Negative Electron Resists," *Polymer Engg. Sci.*, **14**, 529 (1974).
9-21. Goncher, G. M., J. W. Lyngdal, and G. L. Lamer, "Sensitization of Optical Photoresists for Electron-Beam Exposure of Submicron Patterns," *J. Vac. Sci. Technol.*, **B6**, 384 (1988).
9-22. Schlegel, L., and W. Schnabel, "Polymethacrylonitrile as a Resist in X-Ray Lithography," *J. Vac. Sci. Technol.*, **B6**, 82 (1988).
9-23. Shibayama, K., and T. Kato, "Submicron Lithography in Japan," *Polymer Engg. Sci.*, **26**, 1140 (1986).

9-24. Huber, H., H. Betz, and A. Heuberger, "Synchrotron Lithography: The Way to Sub-Micron Features with Single Layer Resists," *Polymer. Engg. Sci.*, **26**, 1153 (1986).
9-25. Brault, R. G., and L. J. Miller, "Sensitivity and Contrast of Some Proton-Beam Resists," *Polymer Engg. Sci.*, **20**, 1064 (1980).

Physical mechanisms associated with polymer dissolution

9-26. Ueberreiter, K., "The Solution Process," in J. Crank, and G. S. Park, eds., *Diffusion in Polymers*, Academic Press, London, 1968, chapter 7.

Mathematical models of the diffusion process

9-27. Lee, P. I., and N. A. Peppas, "Prediction of Polymer Dissolution in Swellable Controlled-Release Systems," *J. Controlled Release*, **6**, 207 (1987).
9-28. Tu, Yo-O., and A. C. Ouano, "Model for the Kinematics of Polymer Dissolution," *IBM J. Res. Develop.*, **21**, 131 (1977).

Measurements of dissolution rates

9-29. Rodriguez, F., P. D. Krasicky, and R. J. Groele, "Dissolution Rate Measurements," *Solid State Technol.*, **28**(5), 125 (1985).
9-30. Krasicky, P. D., R. J. Groele, J. A. Jubinsky, F. Rodriguez, Y. M. N. Namaste, and S. K. Obendorf, "Studies of Dissolution Phenomena in Microlithography," *Polymer Engg. Sci.*, **27**, 282 (1987).
9-31. Cooper, W. J., P. D. Krasicky, and F. Rodriguez, "Dissolution Rates of Poly(Methyl Methacrylate) Films in Mixed Solvents," *J. Appl. Polymer Sci.*, **31**, 65 (1986).

Energy absorption in a resist and simulation of resist profiles during development

9-32. Greeneich, J. S., "Solubility Rate of Poly-(Methyl Methacrylate), PMMA, Electron-Resist," *J. Electrochem. Soc.*, **121**, 1669 (1974).
9-33. Greeneich, J. S., and T. van Duzer, "An Exposure Model for Electron-Sensitive Resists," *IEEE Trans. Electr. Dev.*, **21**, 286 (1974).
9-34. Greeneich, J. S., "Time Evolution of Developed Contours in Poly-(Methyl Methacrylate) Electron Resist," *J. Appl. Phys.*, **45**, 5264 (1974).
9-35. Greeneich, J. S., "Developer Characteristics of Poly-(Methyl Methacrylate) Electron Resist," *J. Electrochem. Soc.*, **122**, 970 (1975).
9-36. Jewett, R. E., P. I. Hagouel, A. R. Neureuther, and T. van Duzer, "Line-Profile Resist Development Simulation Techniques," *Polymer Engg. Sci.*, **17**, 381 (1977).
9-37. Watts, M. P. C., "Analytical Model of Positive Resist Development Applied to Linewidth Control in Optical Lithography," *J. Vac. Sci. Technol.*, **B3**, 434 (1985).
9-38. Everhart, T. E., and P. H. Hoff, "Determination of Kilovolt Electron Energy Dissipation vs Penetration Distance in Solid Materials," *J. Appl. Phys.*, **42**, 5837 (1971).
9-39. Kyser, D. F., and N. S. Viswanathan, "Monte Carlo Simulation of Spatially Distributed Beams in Electron-Beam Lithography," *J. Vac. Sci. Technol.*, **12**, 1305 (1975).

Fluid dynamics of spin coating of nonvolatile liquids

9-40. Emslie, A. G., F. J. Bonner, and L. G. Peck, "Flow of a Viscous Liquid on a Rotating Disk," *J. Appl. Phys.*, **11**, 963 (1966).
9-41. Washo, B. D., "Rheology and Modeling of the Spin Coating Process," *IBM J. Res. Develop.*, **21**, 190 (1977).
9-42. Acrivos, A., M. G. Shah, and E. E. Petersen, "On the Flow of a Non-Newtonian Liquid on a Rotating Disk," *J. Appl. Phys.*, **31**, 963 (1960).

Effect of solvent evaporation

9-43. Flack, W. W., D. S. Soong, A. T. Bell, and D. W. Hess, "A Mathematical Model for Spin Coating of Polymer Resists," *J. Appl. Phys.*, **56**, 1199 (1984).
9-44. Chen, B. T., "Investigation of the Solvent-Evaporation Effect on Spin Coating of Thin Films," *Polymer Engg, Sci.*, **23**, 399 (1983).

Critical examination of the approximation inherent in earlier studies of spin coating

9-45. Jenekhe, S. A., "Effects of Solvent Mass Transfer on Flow of Polymer Solutions on a Flat Rotating Disk," *IEC Fund.*, **23**, 425 (1984).

Experimental and theoretical treatment of the planarization problem

9-46. White, L. K., "Planarization Properties of Resist and Polyimide Coatings," *J. Electrochem. Soc.*, **130**, 1543 (1983).
9-47. White, L. K., and N. Miszkowski, "Topography-Induced Thickness Variation Anomalies for Spin-Coated, Thin Films," *J. Vac. Sci. Technol.*, **33**, 862 (1985).
9-48. White, L. K., "Approximating Spun-On, Thin Film Planarization Properties on Complex Topography," *J. Electrochem. Soc.*, **132**, 168 (1985).
9-49. Wilson, R. H., and P. A. Piacente, "Effect of Circuit Structure on Planarization Resist Thickness," *J. Electrochem. Soc.*, **133**, 981 (1986).
9-50. Stillwagon, L. E., and R. G. Larson, "Fundamentals of Topographic Substrate Leveling," *J. Appl. Phys.*, **63**, 5251 (1988).
9-51. Daughton, W. J., and F. L. Givens, "An Investigation of the Thickness Variation of Spun-On Thin Films Commonly Associated with the Semiconductor Industry," *J. Electrochem. Soc.*, **129**, 173 (1982).

Recent study of spin coating

9-52. Rehg, T. J., and B. G. Higgins, "Spin Coating of Colloidal Suspensions," *AIChEJ*, **38**, 489 (1992).